



TECHNISCHE UNIVERSITÄT CHEMNITZ

Faculty of Electrical Engineering and Information Technology

Research Project

VALIDITY ANALYSIS OF SAFETY SETS APPLIED IN TRANSIENT STABILITY OF POWER GRIDS

Gyula Molnár

Supervisors: M. Sc. Tim Aschenbruck
Dr. Willem Esterhuizen

Examinor: Prof. Dr.-Ing. habil. Stefan Streif

Date: August 27th 2021



Automatic Control and System Dynamics
Prof. Dr.-Ing. habil. Stefan Streif

KURZFASSUNG

Das Thema dieses Forschungsprojektes fokussiert sich auf die mengenbasierte Analyse der transienten Rotorwinkelstabilität in Stromversorgungssystemen. An diesem Themenbereich wurde in der kürzeren Vergangenheit intensive Forschung betrieben, da die mengenbasierte Analyse als theoretischer Rahmen dient, in dem ein komplexes Stromnetz durch begrenzte Entkopplungsvariablen in kleinere Teilsysteme zerlegt werden kann. Auf diese Weise kann die Analyse zerlegter Netzelemente separat durchgeführt, und schließlich eine Aussage über das Gesamtsystem getroffen werden.

Dieses Forschungsprojekt untersucht zunächst die Grundlagen der Stabilität von Stromversorgungsnetzen, der Stromnetzmodellierung, der Barrierentheorie, der Netzentkopplung und der mengenbasierten Analyse unter Verwendung der Barrierentheorie. Die Arbeit beschäftigt sich ferner mit der Mengengültigkeitsanalyse für zulässige, und robuste invariante Mengen, und legt schließlich eine Konjektur über die Existenz von Barrierephasen fest. Anschließend folgt eine Untersuchung der Barrierephasen im Zusammenhang mit der Konsistenz der Mengen sowie die Plausibilität zur Entwicklung eines iterativen Algorithmus, der diese Phasen als Basis verwenden würde, um mengenbasierte transiente Stabilitätsanalyse zu automatisieren.

ABSTRACT

The main topic of this research project focuses on set-based transient rotor angle stability of power systems. This topic area has been subject to extensive research recently, as set-based analysis serves as a theoretical framework in which a complex power network can be decomposed into smaller subsystems through a bounded decoupling variable. This way, analyses of decomposed power system elements can be conducted individually, eventually incorporating them into a statement about the whole system's stability.

This research project initially explores the fundamentals of power system stability, power grid modeling, the theory of barriers, grid decoupling, and set based analysis utilizing the theory of barriers. The work further engages in discussing set-validity analysis for admissible-, and robust invariant sets, arriving at a conjecture proposing the existence of barrier phases. Subsequently, further exploration of what barrier phases imply about set validity, and whether it would be plausible to develop an iterative algorithm utilizing them to automate of set-based transient stability analysis is carried out.

CONTENTS

NOTATION	IV
LIST OF ABBREVIATIONS	VI
LIST OF FIGURES	VII
LIST OF TABLES	VIII
1 THEORETICAL BACKGROUND	1
1.1 Power Systems Stability	1
1.1.1 Transient Stability	2
1.1.2 Approaches for Stability Assessment	5
1.2 Power System Modeling	11
1.2.1 Coupled Oscillator Representation	13
1.3 Viability Theory and Theory of Barriers	15
1.3.1 Theory of Barriers	18
1.4 Power Grid Decoupling for Set-Based Analysis	20
1.5 Determining Set Barriers for Power Grid Analysis	24
2 SET-VALIDITY ANALYSIS OF BARRIER TRAJECTORIES FOR ADMISSIBLE AND ROBUST INVARIANT SETS IN POWER SYSTEMS	26
2.1 Validity of MRPI Sets	26
2.1.1 Constraint Violation	29
2.1.2 Jumping Phenomenon	29
2.2 Research Framework Setup	32
2.3 Interactive Slider	34
2.4 Observation on Barrier Phases	36
2.5 Barrier phases and set validity	42
2.6 Iterative approach towards finding consistent MRPI sets	44
2.7 Inverse damping adjustment	49
3 CONCLUSION AND OUTLOOK	51
3.1 Summary	51
3.2 Outlook	52
BIBLIOGRAPHY	53

NOTATION

A	Node MRPI area
A_i	Power output / power demand of the i th node
\mathcal{A}	Admissible set
$[\partial\mathcal{A}]_-$	Admissible set barrier
\mathbf{c}	Combined node dynamics vector
D_i	Damping constant of the i th node
\mathcal{D}	Disturbance space
\mathbf{d}	Disturbance input
$\bar{\mathbf{d}}$	Input corresponding to the barrier trajectory
δ	Torque angle or angular deviation
$\delta_{\min}, \delta_{\max}$	Angular constraints boundaries
δ_{sat}	Saturated torque angle
E_i^*	Steady-state internal voltage of the i th node
$\mathbf{f}(\cdot)$	System dynamics
$f_{G,i,j}$	The i th component of the dynamics of the j th generator node
$f_{L,i,j}$	The i th component of the dynamics of the j th load node
$\Phi(\cdot)$	Continuous feedback control law
Γ	Set of all generator nodes
\mathcal{G}	Constraint set
\mathcal{G}_0	Constraint boundary set
\mathcal{G}_-	Constraint internal set
γ_{ij}	Phase shift involved in the coupling between nodes i and j
$g_i(\cdot)$	Constraint function of the i th constraint
H_i	Inertia constant of the i th node
$\mathbf{h}(\cdot)$	System output function
\mathbf{I}	Current injection vector
i_{ref}	Index of the reference node
K_{ij}	Strength of dynamical coupling between nodes i and j
Λ	Set of all load nodes
$\bar{\boldsymbol{\lambda}}$	Adjoint vector
$\boldsymbol{\lambda}_{-,i}$	Lower adjoint evolution

$\lambda_{\sim,i}$	Upper adjoint evolution
M	Angular momentum
\mathcal{M}	Maximal robust positively invariant (MRPI) set
$[\partial\mathcal{M}]_{-}$	MRPI set barrier
N	Number of machines/nodes/oscillators in the system
\mathcal{N}_i	Set of the i th node's neighboring nodes
ω, ω_R	Frequency or rotation speed, reference frequency
P_i^*	Steady-state active power injection of the i th node
P_s, P_e, P_a	Shaft-, electrical-, and accelerating power
ρ	Number of state-space constraints
Θ_i	Oscillator phase of the i th oscillator
\bar{t}	Time of angular constraint boundary intersection
$\bar{t}_{\sim,i}$	Time of the lower barrier candidate's tangential intersection of the higher constraint boundary.
$\bar{t}_{\sim,i}$	Time of the upper barrier candidate's tangential intersection of the lower constraint boundary.
\tilde{t}	Time of the first $\omega = 0$ axis intersection
\mathcal{U}	State-dependent control space
\mathbf{u}	Control input
\mathcal{X}	State space
$X(\cdot)$	Phase-dependent influence
\mathbf{x}	State vector
$\bar{\mathbf{x}}$	Initial state on the admissible-, or MRPI barrier
\mathbf{x}_{eq}	State vector at equilibrium
$\mathbf{x}_{\bar{d},\bar{\mathbf{x}}}, \mathbf{x}_{\bar{d}}$	Barrier trajectory with initial conditions $\bar{\mathbf{x}}$ and $\mathbf{b}ard$
$\mathbf{x}_{\sim,i}$	Lower candidate trajectory
$\mathbf{x}_{\sim,i}$	Upper candidate trajectory
\mathcal{Y}	Output space
\mathbf{Y}	Nodal admittance matrix
\mathbf{y}	Output vector
y_{ij}	Admittance between nodes i and j
y_{ij}	Admittance between nodes i and j
\mathbf{V}	Voltage injection vector
V_i^*	Steady-state terminal voltage of the i th node
\mathcal{Z}	Control space
$Z(\cdot)$	Phase-dependent response
$\bar{\mathbf{z}}$	State of angular constraint boundary intersection

LIST OF ABBREVIATIONS

CCA	Critical Clearing Angle
CCT	Critical Clearing Time
MRPI	Maximal Robust Positively Invariant
RPI	Robustly Positively Invariant

LIST OF FIGURES

Figure 1.1	A simplified classification of Power System Stability.	2
Figure 1.2	Dy-Liacco's diagram.	3
Figure 1.3	Power-angle curve.	6
Figure 1.4	Critical Clearing Angle.	7
Figure 1.5	Time domain power angle plots.	8
Figure 1.6	Visualization of state (in)stability in the sense of Lyapunov.	9
Figure 1.7	Visualization of backward-, and forward reachable sets.	11
Figure 1.8	Huygens' illustration to the double clock experiment.	14
Figure 1.9	Block diagram of a dynamical system.	17
Figure 1.10	Topology of an example power network.	21
Figure 1.11	Dependency graph of an example power network.	22
Figure 1.12	Decomposed dependency graph of an example power system.	23
Figure 2.1	Examples of valid MRPI sets.	27
Figure 2.2	Evolution of the adjoint vector around the jumping point.	28
Figure 2.3	Diagrams of the jumping phenomenon.	28
Figure 2.4	Vectogram along valid set barriers.	31
Figure 2.5	Jumping conditions along the $\omega = 0$ axis.	32
Figure 2.6	The nine-bus test system.	33
Figure 2.7	Quiver plots of the saturated state derivatives.	34
Figure 2.8	Sliders with angular constraint values.	35
Figure 2.9	Stage 1 MRPI barrier phase.	36
Figure 2.10	Stage 2 MRPI barrier phase.	37
Figure 2.11	Stage 3 MRPI barrier phase.	37
Figure 2.12	Stage 4 MRPI barrier phase.	38
Figure 2.13	Stage 5 MRPI barrier phase.	38
Figure 2.14	Stage 6 MRPI barrier phase.	39
Figure 2.15	Stage 7 MRPI barrier phase.	39
Figure 2.16	Stage 8 MRPI barrier phase.	40
Figure 2.17	Topography of the one machine, one bus system.	42
Figure 2.18	Phases in the OMOB system.	43
Figure 2.19	Phase diagrams of the nine-bus system. (Constraint adjust. I.)	45
Figure 2.20	Phase diagrams of the nine-bus system. (Constraint adjust. II.)	46
Figure 2.21	Phase diagrams of the nine-bus system. (Constraint adjust. III.)	47
Figure 2.22	Phase diagrams of the nine-bus system. (Constraint adjust. IV.)	48
Figure 2.23	Phase diagrams of the nine-bus system. (Damping adjustment.)	50

LIST OF TABLES

Table 1.1	Some fields utilizing viability theory.	16
Table 2.1	Characteristics of MRPI barrier candidate trajectory phases.	41
Table 2.2	Initial phases and relevant constraints of MRPI barrier candidates.	45
Table 2.3	Phases of MRPI barrier candidates as in Figure 2.20.	46
Table 2.4	Phases of MRPI barrier candidates as in Figure 2.21.	47
Table 2.5	Phases of MRPI barrier candidates as in Figure 2.22.	48
Table 2.6	The damping coefficient's effect on MRPI barrier phases.	50

THEORETICAL BACKGROUND

The generation of electrical energy and the delivery thereof is an area of electrical engineering that brings along problems that excite many experts, as in our current times, most households and businesses depend on a safe and reliable power source to operate.

However, such a power source presupposes a reliable transmission-, and distribution grid of interoperating electrical equipment. When it comes to reliability, it is inevitable to examine such an electrical network as a whole. Thus, power grid models for simulation and analysis were developed to enable and support power systems management.

1.1 Power Systems Stability

Power systems management is concerned with a safe and reliable power flow in three aspects as described in [18]:

- Power system protection deals with the safe operation of power system equipment, such as transformers, generators, and transmission lines. [18, Part I]
- Power system control has to do with the (economically) optimal operation of the whole power grid, thus involves topics such as energy management, and the unit commitment- and optimal power flow problems. [18, Part III]
- Power system stability is focusing on preserving the integrity of the power grid in that the power system as a whole is able to regain a state of equilibrium after a physical disturbance [18, Part II], and is the part we will be most concerned with in this work.

As described in [23, S. 2.2], it makes practical sense to break the problem of power system stability up into (sometimes overlapping, but more or less distinct) classes and subclasses that are similar in physical nature, the magnitude of the disturbance, in affected devices, processes, or applicable calculation methods. Figure 1.1 serves as a brief overview of this classification.

- Voltage stability is concerned with being able to maintain an acceptable voltage level on all buses after a disturbance has occurred [23, S. 2.1.2]. Voltage stability might be further divided into overlapping subcategories of small- or large disturbance stability as well as short-, and long term stability [18, S. 8.2.3].
- Frequency stability is concerned with the power system's ability to maintain its steady frequency after a major disturbance, resulting in a significant imbalance between power generation and consumption. [18, S. 8.2.4] Such major disturbances

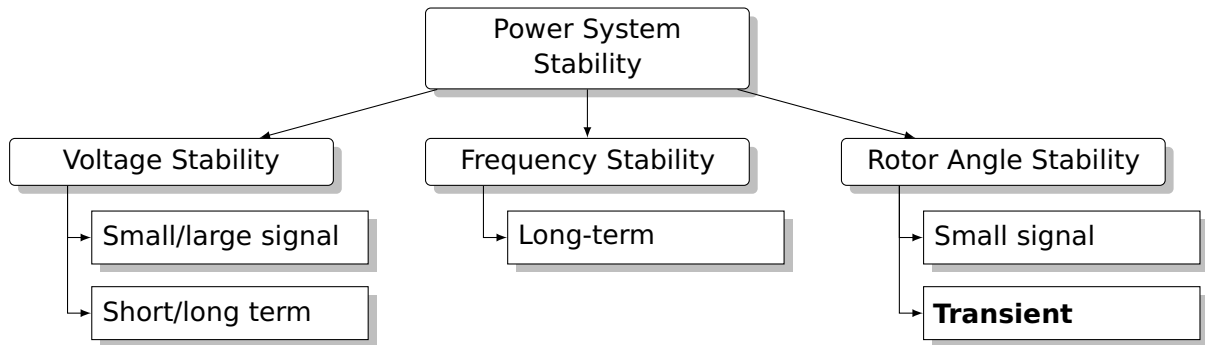


Figure 1.1: A simplified classification of Power System Stability. Adapted from [23].

cause significant deviation of voltages, frequencies, and power flows that require adjusting slow processes and controls (such as boiler-, or conduit dynamics), and so are not included in other models for Power system stability. [23, S. 2.1.3] "Generally, frequency stability problems are associated with inadequacies in equipment responses, poor coordination of control and protection equipment, or insufficient generation reserve." [18, S. 8.2.4]

- Rotor angle stability is concerned with the ability of a power system of interconnected synchronous machines to maintain synchronism, and has to do with studying electromechanical oscillations present in the system. Rotor angle stability may further be subdivided into two subcategories: small signal stability, and transient stability. The former is concerned with the ability of the power system to maintain phase synchronism under continuous disturbances (such as ever-present changes in power generation and consumption) considered small enough for system equations to be linearized, while with the latter the focus is on whether the power system is able to maintain synchronism following a disturbance so severe, that the pre-, and post disturbance steady state of the power system differ significantly. [23, S. 2.1.1] [18, S. 8.2.2]

Of all power system stability classes, this work will be considered with *transient rotor angle stability* exclusively.

1.1.1 Transient Stability

As described above, transient stability analysis deals with fault scenarios in which the pre-, and post-disturbance steady states differ significantly. Speaking of changes in power system steady state it is worth touching on the subject of Operating States as conceptualized in [14] and further studied in [17], according to which, three sets of equations supervise power system operation:

- A set of differential equations describing the physical laws governing the **dynamical behavior** of the system components.
- A set of algebraic equations comprising **equality constraints**, that is, the relationship between power generation and consumption.

- Another set of algebraic equations describing **inequality constraints**, representing constraints on system variables that should not be exceeded.

Since —as described in Section 1.1— power system stability is most concerned with whether and how a power system regains a state of equilibrium after a physical disturbance, it is inequality constraints (again, describing constraints on system variables) that transient stability analysis is most concerned with. However, it is discussed in Section 1.2.1 that system parameters static to the equilibrium state (such as steady-state power consumption or steady-state voltages) are obtained by optimization of equality constraints, as in solving the optimal power flow problem. These steady-state system parameters are taken as constant for the purposes of transient stability analysis (since only very small time scales are considered), and thus are viewed as static input parameters to dynamical models. These dynamical models are then used to describe the evolution of system variables, and to examine if inequality constraints are violated.

Based on whether equality-, and inequality constraints are met, [17] describes five operating states of power system operation as summarized in Figure 1.2.

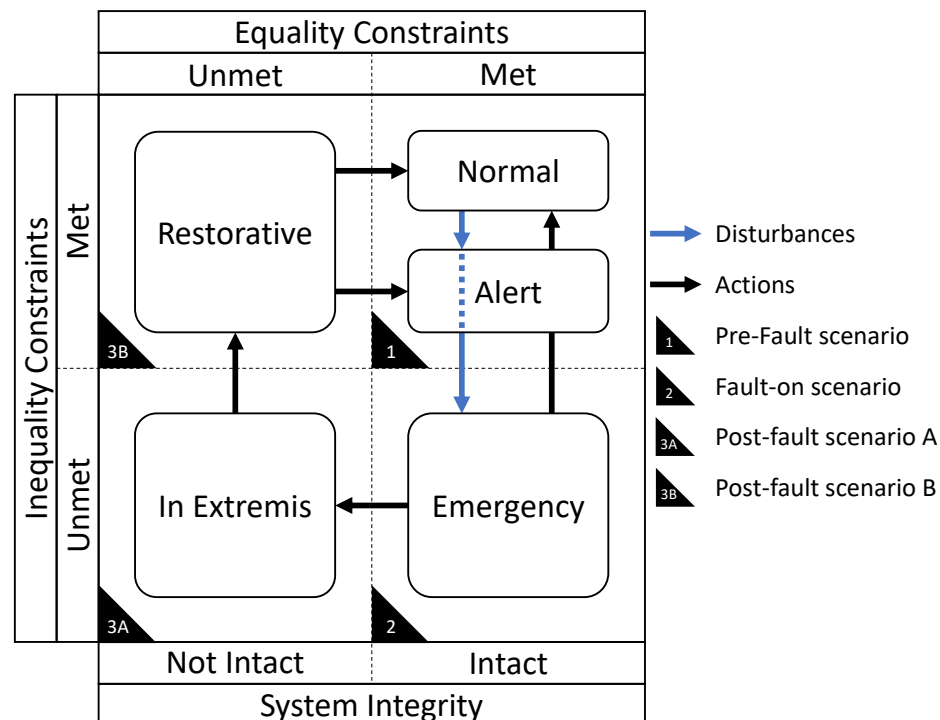


Figure 1.2: Dy-Liacco's diagram extended with possible pre-fault-, fault-on, and post-fault states. Adapted from [17].

During normal operation, all system constraints are met. Once a disturbance causes some system attributes to reach a level of inadequacy, the power system might enter the alert state in which preventive action must be taken to return the system to the normal state of system attributes between adequate thresholds, while constraints are still met all along.

However, a large-scale disturbance might cause the power system to violate one or more inequality (voltage, rotor angle, frequency, ...) constraints, and thus enter the emer-

gency state. Once here, it might be possible to –through fast corrective action– bring the system back to a state of met constraints. This might be achievable due to the possibility to overload an electric component for a short amount of time, that hasn't been exceeded before corrective action was taken.

If components have been overloaded more, or for longer than allowed, built-in physical protection might disable components causing the system to lose integrity, resulting in partial-, or total service interruption, entering the in extremis operating state.

Once inequality constraints are satisfied, the power system enters the restorative state, where resynchronization and load pickup takes place, returning the system to a steady state in which all conditions are met once again.

With transient stability, the scope of the analysis is whether angular-, and frequency constraints are met in a given steady state of power system operation, and how rotor angles and frequencies evolve over time in case of a state transition.

Transient security analysis may be divided into a static and a dynamic part, as summarized in [33, S. 1.3.2]. The static part aims to examine the post-fault equilibrium state of the power system, checking whether it leads to acceptable operating conditions, that is, whether inequality constraints are met. However, a post-fault equilibrium state might not be stable; dynamic transient security assessment considers how the system will reach its post-fault operating conditions.

Thus, in the scope of transient security analysis, three scenarios are always considered:

- The *pre-fault-scenario* considers the pre-fault equilibrium point (the pre-fault steady state), which serves as a starting point for transient analysis. As shown in Figure 1.2, the pre-fault-scenario may correspond to the normal-, or alert operating states, in which inequality constraints remain fulfilled.
- The *fault-on-scenario* considers the system dynamics that have –due to the appearance of a fault– changed. The fault-on-scenario may correspond to the Emergency operating state in which some inequality constraints are being violated.
- The *post-fault-scenario* considers the post-fault equilibrium point, and post-fault inequality constraints after the system dynamics once again underwent a change due to fault isolation or clearance. The post-fault-scenario may either correspond to the in extremis operating state in which –although a number of power system protection measures might took place to avert an emergency– inequality constraints remain unmet, or the restorative operating state in which through additional measures the power system has regained inequality constraint compliance.

Mathematically formulated, the system dynamics in above scenarios can be described through a set of differential equations as in [3, S. 2.1]

$$\begin{aligned}
 \dot{\mathbf{x}} &= \mathbf{f}_I(\mathbf{x}), & t \in]-\infty, t_F[\\
 \dot{\mathbf{x}} &= \mathbf{f}_F(\mathbf{x}), & t \in [t_F, t_C[\\
 \dot{\mathbf{x}} &= \mathbf{f}(\mathbf{x}), & t \in [t_C, \infty[
 \end{aligned} \tag{1.1}$$

where \mathbf{x} is the vector of system state variables, and $f_I(\mathbf{x})$ is the initial system dynamics before a fault occurs at time t_F , referred to as the *pre-fault dynamics* of the system. The *fault-on* dynamics of the system is denoted by $f_F(\mathbf{x})$, prevalent between the fault time t_F and the point in time the fault was cleared, that is, the *clearance time*. The system dynamics after fault clearance is described by $f(\mathbf{x})$.

Transient security analysis' main focus is then to investigate, whether inequality constraints are met in and during transitions between each scenario, as well as to make a statement about the post-fault steady state.

A prototypical use-case for transient stability analysis is critical clearing time (CCT) assessment. Hereby it is assumed that the pre-fault, fault-on, and post-fault dynamics are already assumed as known. Then, one is interested in finding the critical clearing time t_{CC} : the duration up to which the fault dynamics may prevail ($t_C - t_F$) $<$ t_{CC} so that the post-fault dynamics still brings the system to an equilibrium, and so that no inequality constraints are violated during the whole process.

The fault-on scenario may denote a system that is identical to the pre-fault scenario except for the fault, say, a power transmission line being cut, or a short circuit triggering protection equipment. The post-fault dynamics may or may not be identical to the pre-fault one. In the former case, the fault can be considered as resolved, whereas in the latter as detached.

There are multiple methods for computing the critical clearing time. Basically all models discussed in Section 1.1.2 are capable to facilitate CCT calculation. Say, one might rely on the classical model to determine the critical clearing angle using the equal areas criterion, from which the CCT can be obtained if the system frequency is known and taken as constant. Another way would be just running time-domain simulations, while changing the duration of the fault-on dynamics, and examining the results.

1.1.2 Approaches for Stability Assessment

Transient stability analysis is most concerned with the evolution of rotor angles and frequencies of power system components modeled as electrical motors or generators.

Most approaches that are going to be discussed in this subsection build on the classical model of synchronous electrical machines. Although this will only be first introduced in Section 1.2, the following brief overview does not intend to deeply submerge into their theoretical background, and so apprehension should be of no concern.

Equal areas criterion

With the help of (1.4), the equal area criterion can be deduced, which states that

$$\int_{\delta_0}^{\delta_m} P_a d\delta = \int_{\delta_0}^{\delta_m} (P_s - P_e) d\delta \Rightarrow \int_{\delta_0}^{\delta_m} P_s d\delta = \int_{\delta_0}^{\delta_m} P_e d\delta \quad (1.2)$$

where P_s is the shaft-, or mechanical power, P_e is the electrical power, δ_0 is the steady-state torque angle before a fault in the system, and δ_m is the maximal torque angle

that the machine reaches after the fault. Above equation is known as the equal areas criterion of transient power system stability. Figure 1.3 shows (1.5) and the implication of (1.2) in a power-angle diagram.

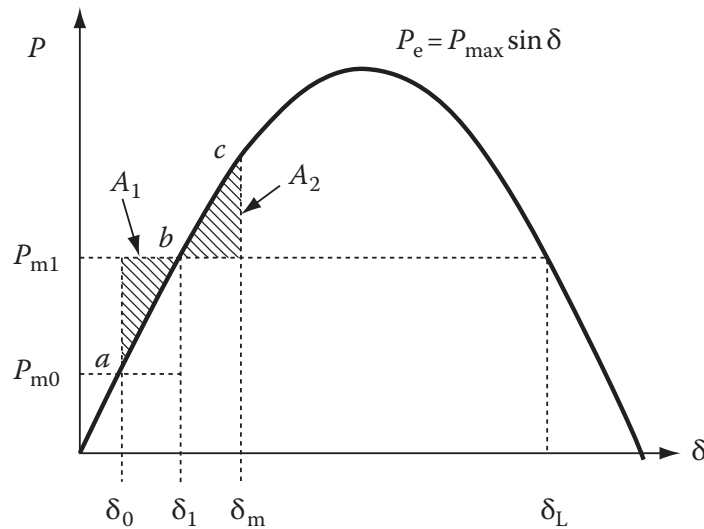


Figure 1.3: Power-angle curve showing a step change in shaft (mechanical) power with areas relevant to (1.2). P_{m0} and P_{m1} are shaft power values (that we annotated as P_s previously) from before-, and after the step change. δ_0 and δ_1 are torque angles associated with steady states corresponding to the aforementioned shaft powers. P_e is the electrical power from (1.5). From [18, Figure 9.5].

The criterion states that since the area under the power-angle curve is (assuming synchronicity) proportional to energy consumed, and since for a machine to maintain its stability, the total (mechanical and electrical) energy generated (or dissipated) during transition from the old equilibrium state δ_0 to the new equilibrium state δ_1 must be equal to the energy dissipated (or generated) during transition from the new equilibrium state δ_1 to the state with the maximum angle deviation δ_m , and so the corresponding areas A_1 and A_2 in the power-angle diagram must also be equal.

This holds intuitively, because assuming that the P_e curve would just be a straight, infinitely long line, say, tangential to the P_e curve in Figure 1.3 at the axis origins, then any step change in mechanical power output would cause the machine to first reach, then *shoot over* the new equilibrium point, oscillating around δ_1 between δ_0 and δ_m until -due to power losses- the oscillation amplitude would settle more and more, and die out eventually.

However, since the $P_e(\delta)$ function is not actually an infinite straight line (neither a machine, nor a bus can generate or consume power above a finite value P_{max}), thus it can very well be, that A_2 simply *can not* get as big as A_1 .

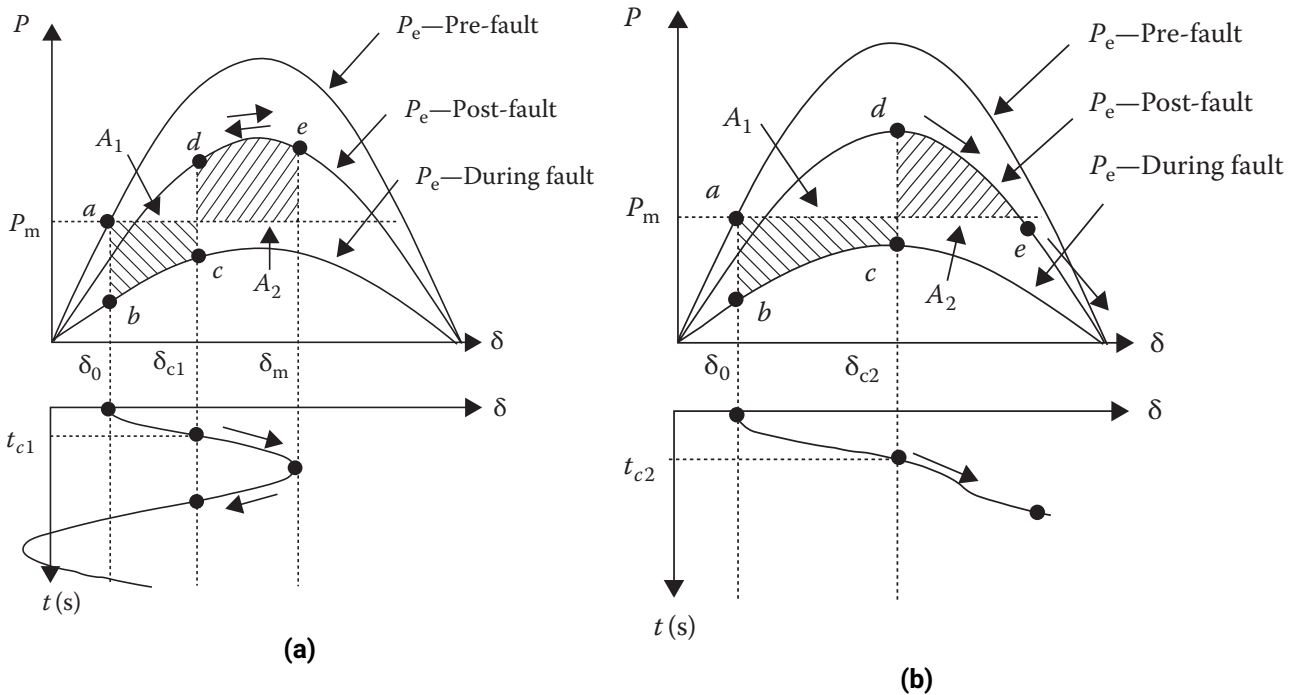


Figure 1.4: Evaluating critical clearing time problems with the help of the power-angle relationship. P_m denotes shaft power, δ_0 the pre-fault steady state torque angle, δ_{c1} the torque angle at the time of fault clearance t_{c1} , and δ_m the maximum torque angle deviance. From [18, Figure 9.6b, Figure 9.7b].

Figure 1.4 shows another use-case for transient stability analysis based on the equal areas criterion, in which power-angle curves corresponding to the fault states (as introduced in Section 1.1.1) are shown. This time it is not the shaft power that is changing from scenario to scenario, but the shape of electrical power-angle curve.

In Figure 1.4(a), the equal areas criterion is met, and the post-fault system will approach its new equilibrium power angle where the line of shaft power P_m intersects the curve of post-fault electrical power P_e .

In Figure 1.4(b), the above criterion is unmet, because the fault was cleared too late for the machine to be able to recover, because there is just *not enough area* between points d and e and curves P_m , and the post-fault P_e for it to match the area proportional to the mechanical energy generated during the fault-on scenario (that is, the area between P_m and P_e during fault and between points b and c .)

Clearly the equal areas method is best applicable in a Single Machine Infinite Bus (SMIB) system. In fact, [18, S. 9.2.3] states that although “*this method is not generally applicable to multimachine systems, it is a valuable learning aid*”.

Other sources, such as [2, S. 2.9] give an example of reducing a two-machine system to a SMIB one, stating that “*the same assumptions used for a system of one machine connected to an infinite bus are often assumed valid for a multimachine system*”, and that this model is “*useful for stability analysis, but is limited to the study of transients for only the ‘first swing’ or for periods on the order of one second*”.

In [27, S. 4.2], the author proposes that “*when a fault occurs in a large power system, only a few machines actively response to the fault and tend to lose synchronism. [...]*

Therefore it is enough to study the behaviour of the critical machines with respect to the rest of the power system in order to evaluate the transient stability of the system for a specific fault”.

However, these works do not anymore count among the newest ones, and as it will shortly be discussed, new or refined models and methods rendered a number of the classical model’s concerns obsolete.

Time-domain simulation

The classical representation of synchronous machines (introduced in Section 1.2) was historically used to reduce the computational burden of more detailed models as in neglecting a number of machine characteristics, such as the effects of damper windings, core saturation, excitation systems, mechanical load dynamics, etc [18, 9.3.1].

However, with today’s cheaply accessible computational capacity, neglecting above properties became unnecessary, as even with more complex, more detailed models, computational methods for time-domain simulation that are efficient enough to produce quasi-instantaneous results (on the short time scale that transient stability analysis is concerned about) are pretty much available.

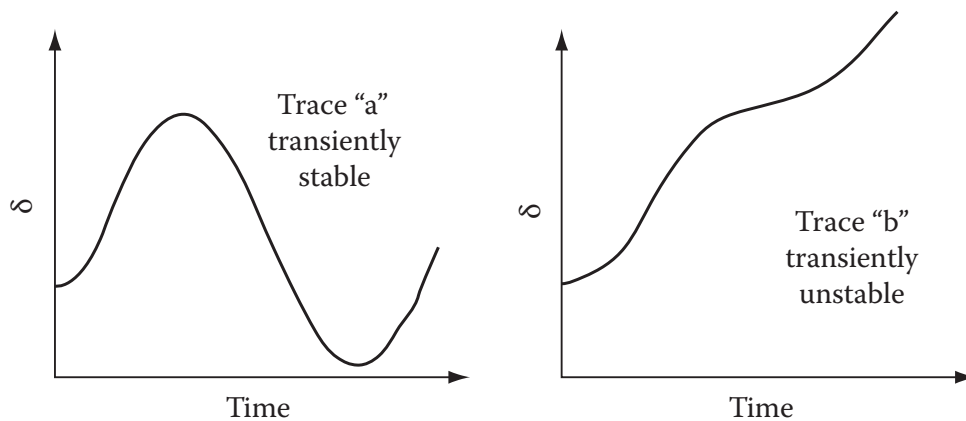


Figure 1.5: Time domain plots of the power angle of a transiently stable-, and unstable machine. From [18, Figure 9.1].

However, classical modeling is still of great use when it comes to analyzing the angular stability of a single machine connected to an infinite bus or, practically, a large network, or when detailed model data is unavailable [18, 9.3.1].

Direct methods

Direct methods of stability analysis seek to provide a statement about transient stability without explicitly solving the set of differential equations describing the dynamical behavior of a system. Indeed, the equal areas criterion was one of the direct methods for transient stability analysis, even though one that is hardly if at all scalable.

The historical overview of direct methods in [18, S. 12.1] emphasizes the importance of the work of Aleksandr Mikhailovich Lyapunov, especially for laying out his second

method for stability (also called the direct method) in [26] way back in 1892. This states that a dynamical system $\dot{\mathbf{x}} = \mathbf{f}(\mathbf{x})$ having an equilibrium point at $\mathbf{x} = \mathbf{0}$ is locally stable around this equilibrium point if there exists a function (a Lyapunov function) $V(\mathbf{x}) : \mathbb{R}^n \rightarrow \mathbb{R}$ such that

$$\begin{aligned}
 V(\mathbf{x}) &= 0 & \text{if } \mathbf{x} &= \mathbf{0} \\
 V(\mathbf{x}) &> 0 & \forall \mathbf{x} &\neq \mathbf{0} \\
 \dot{V}(\mathbf{x}) &\leq 0 & \forall \mathbf{x} &\neq \mathbf{0} & \text{for Lyapunov stability} \\
 \dot{V}(\mathbf{x}) &< 0 & \forall \mathbf{x} &\neq \mathbf{0} & \text{for asymptotic stability} \\
 \dot{V}(\mathbf{x}) &> 0 & \forall \mathbf{x} &\neq \mathbf{0} & \text{for instability}
 \end{aligned} \tag{1.3}$$

Lyapunov stability intuitively means that solutions to the differential equation representing the dynamical system starting *close enough* to (that is, in some finite vicinity around) the equilibrium state, will remain *close enough* to (that is, in some other finite vicinity around) the equilibrium point for all future points in time.

Asymptotic stability intuitively means, that solutions starting *close enough* to (that is, in some finite vicinity around) the equilibrium state will eventually converge towards the equilibrium as time progresses.

Finally, instability means, that the state $\mathbf{x} = \mathbf{0}$ is an unstable equilibrium state, and so that solutions starting anywhere else will eventually leave any vicinity of the equilibrium point.

If a function V satisfies the first two criteria of (1.3), but none of the last three, then Lyapunov's direct method cannot deliver a statement about the systems (in)stability.

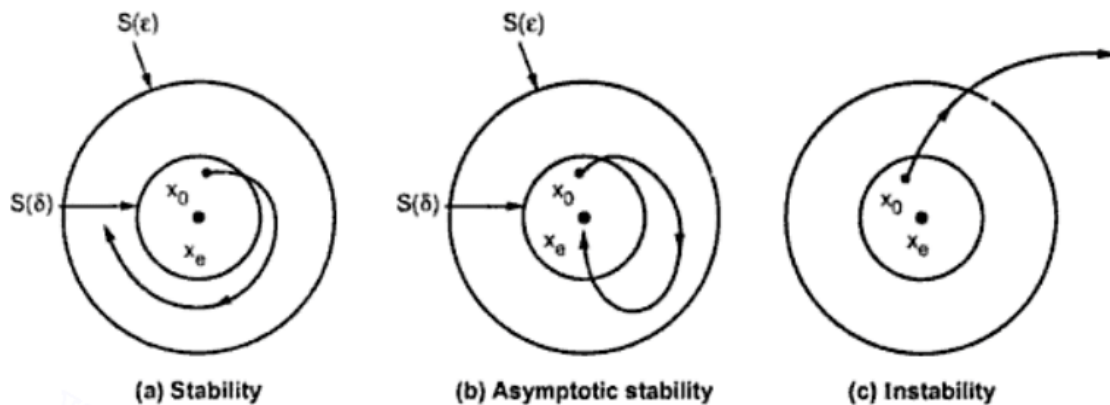


Figure 1.6: Visualization of state (in)stability in the sense of Lyapunov. From [6, Fig. 9.1].

Now, if one starts to wonder what physical meaning could V be assigned to, something like the energy-rotation function of a pendulum might come to mind first. Indeed, an energy function is generally a valid Lyapunov candidate. However, the ingenuity of Lyapunov's method lies in that V can be any $\mathbb{R}^n \rightarrow \mathbb{R}$ function that fulfills (1.3).

However, the major issue with applying Lyapunov's direct method to power systems is that the solutions it delivers are approximated. Literature review in [38] divides scientific analysis of the subject matter in two major parts, with one concentrating on defining the

exact Lyapunov function regardless of the size and complexity of the electric system in question, and the other focusing on defining an equivalent OMIB (one machine, infinite bus) system for a larger power system, as the Lyapunov function for the former is known. Still, both methods rely on approximation: the former because the Lyapunov function can only be expressed in a form of a series that has to be truncated at some point, and the latter because of the simplification that the OMIB model introduces.

Furthermore, [38] cites [33] in proposing that the most successful application of the OMIB-based approach is a hybrid method called SIME (single machine equivalent), which basically applies the OMIB approach and the Lyapunov stability method in each step of a time domain integration, in order to overcome the approximation introduced by the OMIB model. This method is however still way faster than simple time domain integration, as based on the Lyapunov-criteria, a statement about the stability of a trajectory can be made in shorter time.

Model-free approaches

Methods of transient stability analysis discussed so far all rely on white-box models, that is, models that are deterministic, fairly detailed, and rooted in physical knowledge.

Other methods of transient stability analysis are based on gray-, or black-box models, and so rely on raw data more; some sources, such as [1] choose to refer to these methods as model-free instead.

An overview of methods for transient security analysis for power systems was given in [28] in the mid-1990s, dedicating a section to

- Pattern recognition methods, focusing on establishing a functional relationship between selected features of the fault-on trajectory, and the system state.
- Neural net methods, focusing on building and training neural network, that is capable of identifying system state based on a set of selected features.
- Probabilistic methods, focusing on determination of probability distributions for power system stability, e.g. Monte Carlo simulation.
- Expert system methods, combining the knowledge of human experts with other method of transient stability analysis in an "if-then-else" rule set.

Set-based approaches

Since after the millennium, publications discussing the topic of power system transient stability based on reachability analysis started emerging more and more. In [21], reachability analysis is being characterized as focusing on finding reachable sets. These are basically subsets of the state-space of a dynamical system that capture the behavior of entire groups of trajectories at once.

Reachable sets can further be subcategorized into forward-, and backward reachable sets. The former being defined as the set of all states that can be reached along trajectories that start in a specified initial set [21].

A backward reachable set, on the other hand, is the set of states from where trajectories can reach a specified target set [21].

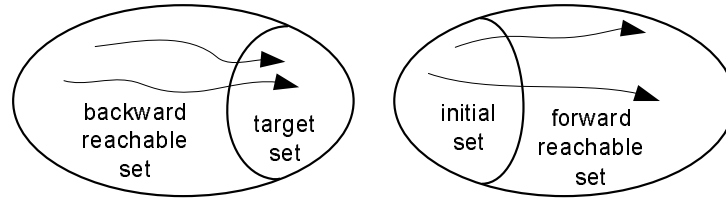


Figure 1.7: Visualization of backward-, and forward reachable sets. From [21, Fig. 1].

The main motivation for the recent academic activity around set-based stability analysis is that it combines advantages of numerical time-domain integration and direct methods. Given a set of initial-, or final states, and sets of disturbances and parameters, all possible trajectories of a system can be computed at once. The result is rigorous, as opposed to those based on Lyapunov's method that are generally -for power systems more complex than OMIB- approximate [1].

However, a significant disadvantage of set-based methods –at least in the case of power system applications– is considerable computational complexity.

As this work is generally focused on set-based power system transient stability analysis, Section 1.3 provides a more detailed overview of the topic area.

1.2 Power System Modeling

A synchronous electrical machine's dynamic behavior is well described by the swing equation [35, Eq. 15.20]

$$M\ddot{\delta} = P_s - P_e = P_a \quad (1.4)$$

where M is the angular momentum, δ is the torque angle or angular deviation (angular difference between the rotor as compared to a reference bus), P_s is the rotor (shaft) power, and P_e is the electrical power. The difference of the latter two, P_a , is called the accelerating power.

The most rudimentary model for synchronous electrical machines used for transient stability analysis considers a generator as a constant voltage behind a transient reactance for electrical parameters, and a mechanical parameter e.g. the moment of inertia such as in (1.4) (or the angular momentum, taken as constant for near-constant angular velocities) [18, 9.3.1]. This is known as the classical model of synchronous electrical machines. As we will soon see in (1.6), the coefficient of the angular acceleration of the machine rotor $\ddot{\delta}$ is often expressed as the function of some inertia constant H and the rated frequency of the machine ω_R . The main correlation governing the classical model is

$$P_e = P_{\max} \sin \delta \quad (1.5)$$

known as the power-angle relationship, where P_e denotes electrical power, P_{\max} is the maximal electrical power, and δ is the torque angle.

In [31], a power grid is modeled as a web of interconnected oscillators –more on coupled oscillator representation in Section 1.2.1– described through a set of swing equations of form

$$\left(\frac{2H_i}{\omega_R} \ddot{\delta}_i + \frac{D_i}{\omega_R} \dot{\delta}_i = A_i - \sum_{j \in \mathcal{N}_i} K_{ij} \cdot \sin(\delta_i - \delta_j - \gamma_{ij}) \right) \forall i \in \Gamma \cup \Lambda \quad (1.6)$$

where

- δ_i is the i th node's angle deviation as compared to a reference node common to the whole system.
- H_i is the i th node inertia constant: $H_i \neq 0 \forall i \in \Gamma$, $H_i = 0 \forall i \in \Lambda$
- ω_R is a reference angular frequency for the system
- D_i is the i th node damping constant
- A_i is the i th node power output / power demand.
- K_{ij} is a constant that represents the strength of the dynamical coupling between the i th and j th node
- γ_{ij} represents a phase shift involved in the coupling between the i th and j th node
- \mathcal{N}_i is the set of all neighboring nodes of the i th node
- Γ is the set of all generator nodes: nodes modeled as second order oscillators, e.g. nodes with $H_i \neq 0$
- Λ is the set of all load nodes: nodes modeled as first order oscillators, e.g. nodes with $H_i = 0$

Notice that (1.4) was also referenced to as the swing equation just before. Indeed, as [29, (2)-(6)] and [31] deduces, (1.6) actually results from linearization of (1.4) around a synchronous equilibrium point and introducing some constants. Said linearization is feasible, since [31]'s main concern is power grid synchronization, and thus considers very short time intervals, and rather small perturbations.

We set out to finding a frequency-synchronous state of all generators of the examined system, so that their angular velocities are equal.

$$\dot{\delta}_i = \dots = \dot{\delta}_n \quad \forall i \in \Gamma \cup \Lambda \quad (1.7)$$

The node with index i_{ref} is considered as a reference bus with a constant reference angle taken as 0, while all the other nodes' state variables

$$\mathbf{x}_i = \begin{bmatrix} x_{1,i} \\ x_{2,i} \end{bmatrix} = \begin{bmatrix} \delta_i \\ \omega_i \end{bmatrix} \quad (1.8)$$

are their angular error δ_i as compared to said reference bus, as well as the derivative thereof $\omega_i = \dot{\delta}_i$ [3, S. 2.2]

$$\omega_{\text{ref}} = \dot{\delta}_{\text{ref}} = \dots = \dot{\delta}_i = \dot{\delta}_{i+1} = \dots = 0 \quad (1.9)$$

Considering said state variables, the equilibrium point is a set of points (generator states)

$$\begin{aligned} \mathbf{x}_{\text{eq},i} &= \begin{bmatrix} x_{\text{eq},1,i} \\ x_{\text{eq},2,i} \end{bmatrix} = \begin{bmatrix} \delta_{\text{eq},i} \\ \omega_{\text{eq},i} \end{bmatrix} = \begin{bmatrix} \delta_{\text{eq},i} \\ \dot{\delta}_{\text{eq},i} \end{bmatrix} = \begin{bmatrix} \delta_{\text{eq},i} \\ 0 \end{bmatrix} \\ \mathbf{x}_{\text{eq}} &= \begin{bmatrix} \mathbf{x}_{\text{eq},1} \\ \mathbf{x}_{\text{eq},2} \end{bmatrix} = \begin{bmatrix} \boldsymbol{\delta}_{\text{eq}} \\ \mathbf{0} \end{bmatrix} \end{aligned} \quad (1.10)$$

so that everything else left unchanged, each and every generator's angular error remains unchanged.

The system dynamic is described by the state's time derivative. Using (1.6):

$$\dot{\mathbf{x}}_i = \begin{bmatrix} \dot{x}_{1,i} \\ \dot{x}_{2,i} \end{bmatrix} = \begin{bmatrix} \dot{\delta}_i \\ \dot{\omega}_i \end{bmatrix} = \begin{bmatrix} \omega_i \\ \frac{\omega_R}{2H_i} \left(A_i - \frac{D_i}{\omega_R} \omega_i - \sum_{j \in \mathcal{N}_i} K_{ij} \cdot \sin(\delta_i - \delta_j - \gamma_{ij}) \right) \end{bmatrix} \forall i \in \Gamma \quad (1.11)$$

$$\dot{\mathbf{x}}_i = \begin{bmatrix} \dot{x}_{1,i} \\ \dot{x}_{2,i} \end{bmatrix} = \begin{bmatrix} \dot{\delta}_i \\ \dot{\omega}_i \end{bmatrix} = \begin{bmatrix} \frac{\omega_R}{D_i} \left(A_i - \sum_{j \in \mathcal{N}_i} K_{ij} \cdot \sin(\delta_i - \delta_j - \gamma_{ij}) \right) \\ 0 \end{bmatrix} \forall i \in \Lambda \quad (1.12)$$

By substituting (1.10) into (1.11) and considering that the very definition of an equilibrium point is that the system dynamic remains zero when evaluated at that point we get:

$$\dot{\mathbf{x}}_{\text{eq},i} |_{\mathbf{x}=\mathbf{x}_{\text{eq}}} = \begin{bmatrix} 0 \\ 0 \end{bmatrix} \quad (1.13)$$

1.2.1 Coupled Oscillator Representation

When observing nature's processes, one need not search long before encountering some kind of periodic phenomena. Such phenomenon was extensively studied by physicists, mathematicians, engineers, and biologists. Arthur Winfree, the author of [40], a professor of theoretical biology himself, went further in that he considered the rhythmical interaction of a whole population of such periodic processes. In his work, he is referencing synchronic phenomena of the human body such as neurons firing in -albeit imperfect- concert, or the chick pacemaker (that is in fact a population of spontaneously beating cells synchronizing to a common frequency). He mentions of multiple studies

reporting on some species of Southeast Asian fireflies who “*tend to flash at regular intervals, but the event can be delayed or triggered precociously by the neighbor flashing*”, resulting in “*whole treefulls of insects flashing synchronously*” [40].

However, research around synchronization phenomena is all but new. It is attributed to 17th century Dutch polyhistor Christiaan Huygens to have first recorded a similar phenomenon within a mechanical system, which he referred to as “odd sympathy” of two pendulum clocks hung from a common rigid beam.

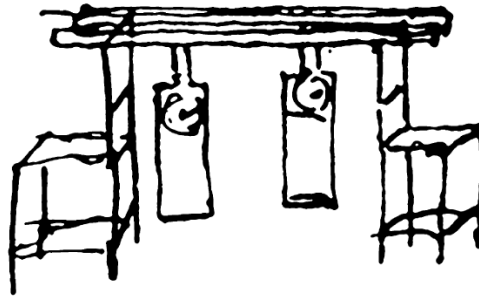


Figure 1.8: Huygens’ original drawing describing his experiment. From [20].

Indeed he observed that the clocks’ pendulums synchronized to each other after some time, no matter their initial start conditions. Even though he initially assumed this was due to the the air currents between the two pendulums, he later concluded that it was actually the tiny, imperceptible motion of the beam that led to the sympathy [11] [20].

Other physical examples include pedestrians’ eventually walking in step with each other on a bridge [36], or how moons revolving around a common planet eventually synchronize so that their orbital periods are integer multiples of that of the moon with the fastest orbital frequency (i.e. moons of a planet tend to line up at regular intervals) [34].

Further examples for synchronization exist in a wide range of disciplines, such as the Belousov-Zhabotinsky reaction in chemistry [41], or a theater audience’s clapping *spontaneously* turning rhythmical [30].

Nonetheless, Winfree proposed a model in [40] that supposed interplay of oscillators “*coupled to the collective rhythm generated by the whole population*” [37]:

$$\dot{\theta}_i = \omega_i + \left(\sum_{j=1}^N X(\theta_j) \right) Z(\theta_i) \quad \forall i \in \{1 \dots N\} \quad (1.14)$$

where θ_i and ω_i are the phase and natural frequency of oscillator i , and N is the number of oscillators, $X(\theta_j)$ is the phase-dependent influence of the j th oscillator on all other oscillators, and $Z(\theta_i)$ is the phase-dependent response or sensitivity function of the i th oscillator.

Winfree’s proposition made a deep impression on physicist Yoshiki Kuramoto, whose refinement of the model –now known as the Kuramoto model– first appeared in [24], although often revisited in further works of his. The popular form of the Kuramoto model is

$$\dot{\theta}_i = \omega_i + \frac{K}{N} \sum_{j=1}^N \sin(\theta_j - \theta_i) \quad \forall i \in \{1 \dots N\} \quad (1.15)$$

where $K \geq 0$ is the coupling strength between oscillators, and the rest is same as in (1.14). However, this form corresponds to the simplest possible case of equally weighted, global (all-to-all), purely sinusoidal coupling. The most general form of the Kuramoto model is

$$\dot{\theta}_i = \omega_i + \sum_{j=1}^N \Gamma_{ij}(\theta_j - \theta_i) \quad \forall i \in \{1 \dots N\} \quad (1.16)$$

where Γ_{ij} is an interaction function of oscillators i and j .

It was in [16] that the applicability of the Kuramoto model to the utility power grid was considered. It was concluded, that in the presence of bimodal distribution of generator/motor frequencies (the bimodality is due to the fact that positive and negative power consumption i.e. generators as well as loads -modeled as synchronous motors in [16]- exist in the grid) and in the case of global coupling (i.e. all-to-all coupling with heterogeneous weights of 1) the synchronization will occur for large enough coupling K . Furthermore it has been predicted that for the underdamped Kuramoto model the synchronization is hysteric. That is, increasing the coupling K leads to phase lock at a K value higher than the K value at which the synchronization ceases as K is decreased.

Even though [16] restrained to a model of global coupling, more papers around power grid synchronization emerged since then, some proposing different models. It was in the 2015 paper [31] that a comparative analysis of power grid synchronization models existing by then has been published. Said paper was deemed timely by the authors, as up to that point, the *“problem of how large scale network structure influences the collective dynamics in power grids”* remained unexplored, even though the availability of powerful data processing tools and substantial computing power was *“making it possible to address large-scale properties of power-grid systems”* [31]. Cited paper compares three leading network structure models on the basis of a coupling model that *“can be regarded as a second-order analog of the Kuramoto model with arbitrary coupling structure”* [31]. This, in fact, is swing equation (1.6) from Section 1.2.

1.3 Viability Theory and Theory of Barriers

In this work we will be relying on viability theory for transient stability analysis, hence a brief overview of the underlying considerations follows.

The author in [5, S. 1.1.1] derives viability theory from the mathematical formulation of the words attributed to ancient Greek philosopher Democritus:

*“Everything existing in the universe is but the fruit of two qualities:
chance and necessity.”*

insisting that the former (chance) describes some kind of regulation law governing the working principles of a dynamic system, while the latter (necessity) corresponds to

some viability constraints on the system. Examples for what these definitions might mean for a given field of study in particular, are outlined in Table 1.1.

Field	Regulation Laws	Viability Constraints
Control Theory	control (feedback) laws	physical and technological constraints
Economics	"invisible hand"	scarcity constraints
Finance	market laws	value of portfolio
Dynamical Cooperative Games	coalition of players acting on the environment	architecture of the connection network
Population Genetics	genotypes or fitness matrices	ecological constraints
Sociological Sciences	culture, psychological and economical considerations of the individual	laws and cultural codes for the survival of the social organization
Cognitive Sciences	synaptic matrices	rationality assumptions

Table 1.1: Some fields utilizing viability theory (adapted from [5, S. 1.1.2]).

As for the aforementioned mathematical formulation, chances or regulation laws are described in the form of a differential equation, such as the one we introduce in (1.17). The mathematical formulation of constraints will be presented in (1.20).

Let us consider a dynamical system and the corresponding Cauchy-problem from the introduction in [4] (with notation adapted from [8, S. 2] and [13, S. 3]) that is possibly controlled and possibly uncertain:

$$\begin{cases} \dot{\mathbf{x}} = \mathbf{f}(\cdot) \\ \mathbf{x}|_{t=0} = \mathbf{x}_0 \\ \mathbf{y} = \mathbf{h}(\mathbf{x}) \end{cases} \quad (1.17)$$

$$\mathbf{f}(\cdot) = \begin{cases} \mathbf{f}(\mathbf{x}, \mathbf{u}, \mathbf{d}) & \text{for controlled, uncertain systems} \\ \mathbf{f}(\mathbf{x}, \mathbf{u}) & \text{for controlled systems} \\ \mathbf{f}(\mathbf{x}, \mathbf{d}) & \text{for uncertain systems} \\ \mathbf{f}(\mathbf{x}) & \text{for other dynamical systems} \end{cases} \quad (1.18)$$

where

- $\mathbf{x} = \mathbf{x}(t)$ denotes a state vector over state space \mathcal{X}
- $\mathbf{y} = \mathbf{y}(t)$ denotes an output vector over the output space \mathcal{Y} .
- $\mathbf{f}(\cdot)$ is a single valued map from some $(\Omega \subset \mathcal{X}) \rightarrow \mathcal{X}$
- $\mathbf{u} = \mathbf{u}(t) \in \mathcal{U}$ denotes a control input vector over the control space \mathcal{Z} .
- $\mathcal{U} : \mathcal{X} \rightarrow \mathcal{Z}$ is a set valued map representing a state-dependent input constraint.

- $\mathbf{h} = \mathbf{h}(\mathbf{x}) = \mathbf{h}(\mathbf{x}(t))$ denotes the output function of the system.
- $\mathbf{d} = \mathbf{d}(t)$ is an (external) disturbance input vector over the disturbance space \mathcal{D}

with time $t \in [0, T]$ evolving between 0 and an arbitrarily chosen point in time $T \in \mathbb{R}$. Then, as in [4, Def. 1.1.2]:

Definition 1 (Locally viable set). A set $\mathcal{K} \subset \Omega$ is said to be locally viable under $\mathbf{f}(\mathbf{x}(t))$ if

$$\forall \mathbf{x}_0 \in \mathcal{K} \exists T > 0 : \forall t \in [0, T], \mathbf{x}(t) \in \mathcal{K} \text{ and (1.17) has at least one solution.}$$

Definition 2 (Globally viable set). A set $\mathcal{K} \subset \Omega$ is said to be globally viable under $\mathbf{f}(\mathbf{x}(t))$ if it satisfies Def. 1 even in $T = \infty$:

$$\forall \mathbf{x}_0 \in \mathcal{K} : \forall t \in [0, \infty], \mathbf{x}(t) \in \mathcal{K} \text{ and (1.17) has at least one solution.}$$

Definition 3 ([Robustly] Positively invariant set). A set $\mathcal{K} \subset \Omega$ is said to be positively invariant under $\mathbf{f}(\mathbf{x}(t))$ or robustly positively invariant (RPI) under $\mathbf{f}(\mathbf{x}(t), \mathbf{d}(t))$ if it satisfies Def. 2 for all solutions to (1.17):

$$\forall \mathbf{x}_0 \in \mathcal{K} : \forall t \in [0, \infty], \mathbf{x}(t) \in \mathcal{K} \text{ and } \{\mathbf{x}(t), \mathbf{d}(t)\} \text{ always satisfies (1.17)}$$

Definition 4 ([Robustly] Positively controlled invariant set). A set $\mathcal{K} \subset \Omega$ is said to be positively controlled invariant under $\mathbf{f}(\mathbf{x}(t), \mathbf{u}(t))$ or robustly positively controlled invariant under $\mathbf{f}(\mathbf{x}(t), \mathbf{u}(t), \mathbf{d}(t))$ if:

$$\forall \mathbf{x}_0 \in \mathcal{K} : \forall t \in [0, \infty], \mathbf{x}(t) \in \mathcal{K} \text{ and } \{\mathbf{x}(t), \mathbf{u}(t), \mathbf{d}(t)\} \text{ always satisfies (1.17)} \\ \text{and } \exists \mathbf{u}(t) = \Phi(\mathbf{y}(t)) \text{ s.t. Def. 3 holds. [8, Def. 2.3]}$$

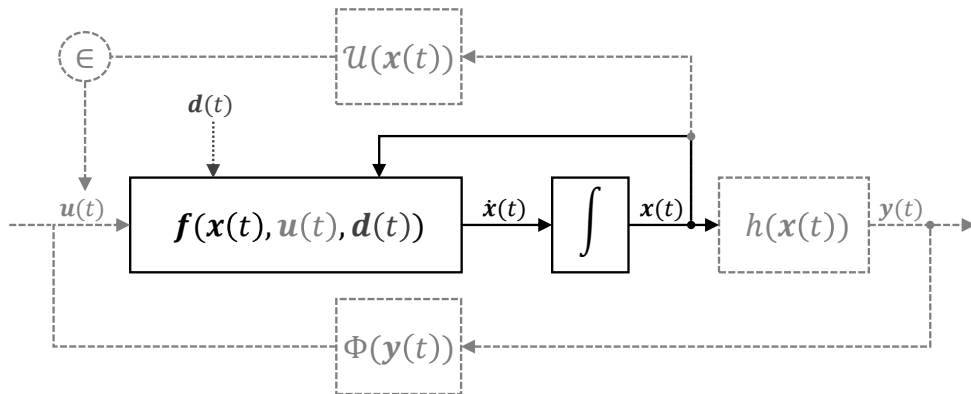


Figure 1.9: Block diagram of a system described in (1.17)-(1.18) and Def. 1-Def. 4.

Above definitions all apply for unconstrained systems. However, for most engineering applications, some constraints are indeed to be considered, be it those derived from physical equipment tolerances or otherwise. Said constraints will be accounted for through a set of real valued constraint functions. For the i th constraint, this function is defined as:

$$g_i(\mathbf{x}(t)) = \begin{cases} g_i(\mathbf{x}(t)) \leq 0 & \text{if the } i\text{th state-space constraint is met} \\ g_i(\mathbf{x}(t)) > 0 & \text{otherwise} \end{cases} \quad (1.19)$$

Then, through extension of (1.17), a constrained system can be described as:

$$\begin{cases} \dot{\mathbf{x}} = \mathbf{f}(\cdot) \\ \mathbf{x}_{t=0} = \mathbf{x}_0 \\ \mathbf{y} = \mathbf{h}(\mathbf{x}) \\ g_i(\mathbf{x}(t)) \leq 0 \forall t \in [0, T], \forall i \in \{1, \dots, p\} \end{cases} \quad (1.20)$$

where p is the number of space-state constraints on the examined system [13, S. 3].

Definition 5 (Constraint set). *The constraint set is the set of all points in \mathcal{X} so that all constraints are met [13, Eq. 3.5]:*

$$\mathcal{G} = \{\mathbf{x}(t) \in \mathcal{X} : g_i(\mathbf{x}(t)) \leq 0 \forall i \in \{1, \dots, p\}\}$$

Definition 6 (Admissible set). *The set of admissible states (or the admissible set) is a set of all initial states in \mathcal{X} for which either an admissible input \mathbf{u} , or disturbance \mathbf{d} exists so that none of the system constraints are violated [13, Eq. 4.1] [3, Def. 1] for all future evolution:*

$$\mathcal{A} = \{\mathbf{x}_0 \in \mathcal{G} : \exists \mathbf{u}(t) \in \mathcal{U} \oplus \exists \mathbf{d}(t) \in \mathcal{D} \text{ s.t. } \mathbf{x}(t) \in \mathcal{G} \forall t \in [0, \infty)\}$$

Since $\mathcal{G} \subset \mathcal{X}$ as per Def. 5, and $\mathcal{K} \subset \Omega \subset \mathcal{X}$, all elements in the admissible set \mathcal{A} are also globally viable under $\mathbf{f}(\mathbf{x}(t))$ as of Def. 2. Accordingly, the admissible set is also referred to as the viability kernel in some sources.

Definition 7 (Maximal robust positively invariant set). *The maximal robust positively invariant set (MRPI) is the union of all RPIs [3, Def. 3] as in Def. 3. Intuitively, it is the set of all initial states in \mathcal{X} for which no future input or disturbance evolutions violate any system constraints:*

$$\mathcal{M} = \{\mathbf{x}_0 \in \mathcal{G} : \mathbf{x}(t) \in \mathcal{G} \forall \mathbf{u}(t) \in \mathcal{U} \oplus \forall \mathbf{d}(t) \in \mathcal{D}, \forall t \in [0, \infty)\}$$

The main motive of what follows revolves around applying the considerations outlined in this subsection to the dynamical system modeling a power grid, specifically finding admissible and invariant sets as a means of making a statement about power grid stability.

1.3.1 Theory of Barriers

Having defined the Admissible set in Def. 6 and the MRPI set in Def. 7, the question remains of how one determines what exact points of the state-space fall inside or outside these sets, given specific system dynamics. In answering this question, we will be relying on the theory of barriers, and the works of [3, S. 3.1], [15, S. 4], and [13].

Let us consider an uncertain dynamical system $\mathbf{f}(\mathbf{x}(t), \mathbf{d}(t))$ from (1.17) and (1.18) that is subject to constraints as in (1.19). We supplement the constraint set \mathcal{G} from Def. 5 with the following sets:

Definition 8 (Constraint boundary set).

$$\mathcal{G}_0 = \{\mathbf{x}(t) \in \mathcal{X} : g_i(\mathbf{x}(t)) = 0 \forall i \in \{1, \dots, p\}\}$$

Definition 9 (Constraint internal set).

$$\mathcal{G}_- = \{\mathbf{x}(t) \in \mathcal{X} : g_i(\mathbf{x}(t)) < 0 \forall i \in \{1, \dots, p\}\}$$

with $\mathcal{G} = \mathcal{G}_0 \cup \mathcal{G}_-$.

We impose assumptions from [3, S. 3.1], [15, S. 4], and [13] as follows:

- (A1) Given that D is compact and convex set, function $\mathbf{d} \in D$ is a Lebesgue measurable function s.t. $\mathbf{d}(t) : [t_0, \infty) \rightarrow D$.
- (A2) Function \mathbf{f} is C^2 with respect to $\mathbf{d} \in D$, and for every \mathbf{d} in an open subset containing D , the function \mathbf{f} is C^2 with respect to $\mathbf{x} \in \mathcal{X}$.
- (A3) There exists a constant $0 < c < +\infty$ such that the following inequality holds:

$$\sup_{\mathbf{d} \in D} |\mathbf{x}^T \mathbf{f}(\mathbf{x}, \mathbf{d})| \leq c(1 + \|\mathbf{x}\|^2)$$

- (A4) The set $\mathbf{f}(\mathbf{x}, D) = \{\mathbf{f}(\mathbf{x}, \mathbf{d}) : \mathbf{d} \in D\}$ is convex for all $\mathbf{x} \in \mathcal{X}$.
- (A5) Function $g_i \forall i \in \{1, 2, \dots, p\}$ is C^2 with respect to $\mathbf{x} \in \mathcal{X}$, and \mathcal{G}_0 defines a manifold.

Given that above assumptions hold, the admissible set \mathcal{A} and the MRPI set \mathcal{M} are closed. Thus we proceed by denoting their boundaries as $\partial\mathcal{A}$ and $\partial\mathcal{M}$, based on which we further define the following barriers:

Definition 10 (Admissible set barrier).

$$[\partial\mathcal{A}]_- = \partial\mathcal{A} \cap \mathcal{G}_-$$

Definition 11 (MRPI set barrier).

$$[\partial\mathcal{M}]_- = \partial\mathcal{M} \cap \mathcal{G}_-$$

Under the assumptions (A1) - (A5), and according to [3, (5)-(9)], [15, Theorem 1.], and [13, Theorem 7.1.], for every initial condition $\bar{\mathbf{x}} \in [\partial\mathcal{M}]_-$ (or $\bar{\mathbf{x}} \in [\partial\mathcal{A}]_-$), there exists an input $\bar{\mathbf{d}} \in D$ such that the resulting trajectory $\mathbf{x}_{\bar{\mathbf{d}}, \bar{\mathbf{x}}}(t) \in [\partial\mathcal{M}]_-$ (or $\mathbf{x}_{\bar{\mathbf{d}}, \bar{\mathbf{x}}}(t) \in [\partial\mathcal{A}]_-$) remains on the MRPI barrier (or admissible set barrier) until the integral curve intersects \mathcal{G}_0 .

Furthermore, $\mathbf{x}_{\bar{\mathbf{d}}}(t) = \mathbf{x}_{\bar{\mathbf{d}}, \bar{\mathbf{x}}}(t)$ and $\bar{\mathbf{d}}$ satisfies the following conditions:

1. There exists a nonzero absolutely continuous maximal solution $\boldsymbol{\lambda}_{\bar{\mathbf{d}}}(t)$ to the adjoint equation

$$\begin{aligned} \dot{\boldsymbol{\lambda}}_{\bar{\mathbf{d}}}(t) &= - \left(\frac{\partial \mathbf{f}}{\partial \mathbf{x}}(\mathbf{x}_{\bar{\mathbf{d}}}(t), \bar{\mathbf{d}}(t)) \right)^T \boldsymbol{\lambda}_{\bar{\mathbf{d}}}(t) \\ \boldsymbol{\lambda}_{\bar{\mathbf{d}}}(\bar{t}) &= \max_{i \in \mathcal{I}} \nabla g_i(\mathbf{z}) \mathbf{f}(\mathbf{z}, \bar{\mathbf{d}}(\bar{t}))^T \end{aligned} \quad (1.21)$$

such that

$$\text{for } [\partial\mathcal{A}]_- : \min_{\mathbf{d} \in \mathcal{D}} \{(\boldsymbol{\lambda}_{\bar{\mathbf{d}}}(t))^T \mathbf{f}(\mathbf{x}_{\bar{\mathbf{d}}}(t), \mathbf{d})\} = 0 \quad (1.22)$$

$$\text{for } [\partial\mathcal{M}]_- : \max_{\mathbf{d} \in \mathcal{D}} \{(\boldsymbol{\lambda}_{\bar{\mathbf{d}}}(t))^T \mathbf{f}(\mathbf{x}_{\bar{\mathbf{d}}}(t), \mathbf{d})\} = 0 \quad (1.23)$$

where $\mathcal{I}(\mathbf{x}) : \{i \in \{1, 2, \dots, p\} : g_i(\mathbf{x}) = 0\}$ is the set of boundary constraints, and \bar{t} is the time at which a point on the constraint $\mathbf{z} \in \mathcal{G}_0$ is reached.

2. The trajectory $\mathbf{x}_{\bar{\mathbf{d}}}(t)$ intersects \mathcal{G}_0 tangentially in point $\mathbf{z} = \mathbf{x}_{\bar{\mathbf{d}}}(\bar{t})$, and so \mathbf{z} is also called the *point of ultimate tangentiality*:

$$\text{for } [\partial\mathcal{A}]_- : \min_{\mathbf{d} \in \mathcal{D}} \max_{i \in \mathcal{I}(\mathbf{z})} \nabla g_i(\mathbf{z}) \mathbf{f}(\mathbf{z}, \mathbf{d}) = 0 \quad (1.24)$$

$$\text{for } [\partial\mathcal{M}]_- : \max_{\mathbf{d} \in \mathcal{D}} \max_{i \in \mathcal{I}(\mathbf{z})} \nabla g_i(\mathbf{z}) \mathbf{f}(\mathbf{z}, \mathbf{d}) = 0 \quad (1.25)$$

Proofs and detailed information on the construction of the admissible-, and MRPI set barriers can be found in [15, S. 4] and [13].

1.4 Power Grid Decoupling for Set-Based Analysis

Although several models of power grids exist [29][2][7][16], physical arrangement dictates that a common trait of these is that they generally assign system components (modeled as oscillators) to nodes-, and connections to edges of a mathematical graph.

This usually results in a large scale system where each node's state is governed by the swing equation as introduced in Section 1.1.2.

However, since...

- ... every node's current state is characterized by state variable vector (1.8), and...
- ...every node is governed by swing equation (1.4) (torque angle deviation and accelerating power are interdependent), and...
- ...every node's torque angle has to be more or less synchronized to that of adjacent nodes (inequality constraints must be fulfilled), and...
- ...every node's power generation and demand has to be on par with those of adjacent nodes (equality constraints must be fulfilled), and...
- ...every node's state is interdependent to that of any other node's in the model, even if through intermediary nodes (the system is of nonlinear nature), ...

...relying directly on a power grid model for simulation involves solving the swing equations for all the state vectors for each and every time step. In other words, if all n nodes' state vectors are of dimension \mathbb{R}^m , then the state vector of the complete grid model —examined as a whole— would be of dimension $\mathbb{R}^{(n \cdot m)}$.

Other than the computationally challenging task of analyzing nonlinear systems of high-dimensional state spaces, simulation-based approaches also prove to be insufficient due to the possible environmental disturbances characterizing power systems. Furthermore, preliminary safety analysis of a power system requires that all possible states of the system be accounted for [9].

Latter consideration brings us to the sets introduced in Section 1.3. Admissible set \mathcal{A} of Def. 5 and the MRPI set \mathcal{M} of Def. 6 together provide information about a given point \mathbf{x} in state-space as follows [3, S. 3.2]:

$$\mathbf{x} : \begin{cases} \text{safe if } \mathbf{x} \in \mathcal{M} \\ \text{potentially safe if } \mathbf{x} \in \mathcal{A} \setminus \mathcal{M} \\ \text{unsafe if } \mathbf{x} \in \overline{\mathcal{A}} \end{cases} \quad (1.26)$$

However, obtaining \mathcal{A} and \mathcal{M} for high-dimensional nonlinear systems is often difficult, or possible only with certain trade-offs [9].

Thus, decomposing high-dimensional systems into smaller subsystems is desirable, like how [3] applies the decomposition principles introduced in [10], [25] to a power system. Decomposition in aforementioned works follows the principle of considering subsets of the complete system's state vector as a state vector of a smaller system. However, some state variables in these subsystems' state vectors might depend on other state variables of the *big* composed system that might have been decomposed into another subsystem. Such interdependencies between subsystems are accounted for by assigning each state variable to exactly one subsystem as state variable, and considering the variable in question as a disturbance input in other, interdependent subsystems. Said disturbance inputs are also called *decoupling variables* [3] in this context.

Let us take a look at a power system consisting of generators G_1, G_2, G_3 (the latter considered as the reference node) and load L_4 that are all cross-connected as in Figure 1.10.

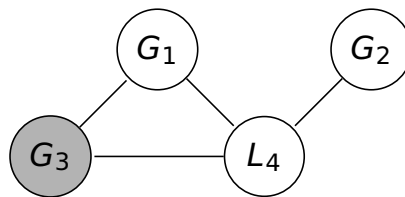


Figure 1.10: Topology of the example four-node network. The colored node denotes the reference generator.

The current state of non-reference nodes G_i and L_i are described by (1.8), and the system dynamics by (1.11) and (1.12):

$$\dot{\mathbf{x}} = \begin{bmatrix} \dot{\mathbf{x}}_1 \\ \dot{\mathbf{x}}_2 \\ \dot{\mathbf{x}}_4 \end{bmatrix} = \begin{bmatrix} (1.11)|_{i=1} \\ (1.11)|_{i=2} \\ (1.12)|_{i=4} \end{bmatrix} = \begin{bmatrix} \dot{\delta}_1 \\ \dot{\omega}_1 \\ \dot{\delta}_2 \\ \dot{\omega}_2 \\ \dot{\delta}_4 \\ \dot{\omega}_4 \end{bmatrix} = \begin{bmatrix} f_{G,1,1}(\omega_1) \\ f_{G,2,1}(\delta_1, \omega_1, \delta_4) \\ f_{G,1,2}(\omega_2) \\ f_{G,2,2}(\delta_2, \omega_2, \delta_4) \\ f_{L,1,4}(\delta_4, \delta_1, \delta_2) \\ 0 \end{bmatrix} \quad (1.27)$$

Notice how δ_3 is not included in above equation as although $3 \in \mathcal{N}_1 \cap \mathcal{N}_4$, since G_3 is being considered as the reference node, $\delta_3 \equiv 0$. Generalizing (1.27) to any arbitrary topology, it becomes

$$\begin{aligned} \dot{\mathbf{x}} &= [\dots \ \dot{\mathbf{x}}_i \ \dots]^T = \\ &= \begin{bmatrix} \vdots \\ \begin{cases} (1.11) & \text{if } i \in \Gamma \\ (1.12) & \text{if } i \in \Lambda \end{cases} \\ \vdots \end{bmatrix} = \begin{bmatrix} \vdots \\ \left[\begin{array}{c} f_{G,1,i}(\omega_i) \\ f_{G,2,i}(\delta_i, \omega_i, \{\delta_j \forall j \in \mathcal{N}_i \setminus \{i_{ref}\}\}) \end{array} \right] & \text{if } i \in \Gamma \\ \left[\begin{array}{c} f_{L,1,i}(\delta_i, \{\delta_j \forall j \in \mathcal{N}_i \setminus \{i_{ref}\}\}) \\ 0 \end{array} \right] & \text{if } i \in \Lambda \\ \vdots \end{bmatrix} \quad (1.28) \\ \forall i \in (\Gamma \cup \Lambda) \setminus \{i_{ref}\} \end{bmatrix} \end{aligned}$$

where Γ and Λ are the set of all generator-, and load nodes in the system respectively, \mathcal{N}_i is the set of all neighboring nodes of the i th node, and i_{ref} is the index of the reference node.

The aforementioned state-interdependence can now be represented in a State Dependency Graph, as it was introduced in [25]. Such graphs are shown for the outlined four-node system, as well as the arbitrary case in Figure 1.11.

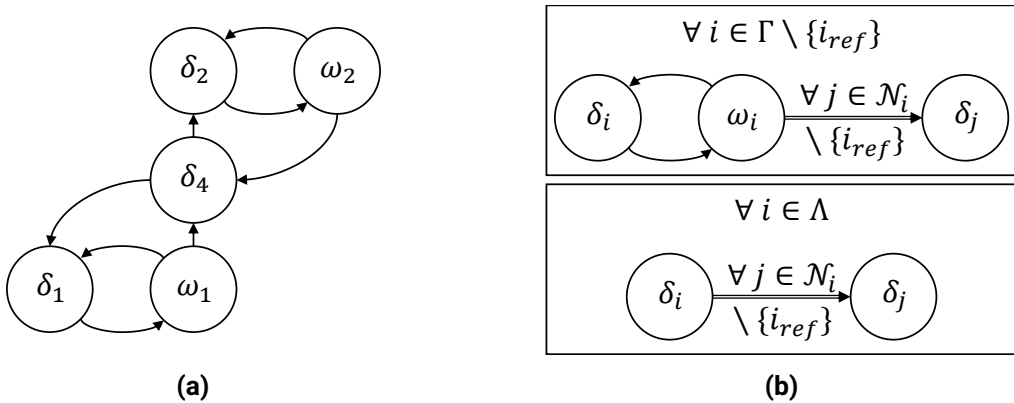


Figure 1.11: Dependency graph for the four-node (a), and the arbitrary case (b).

A convenient decoupling might be treating each node as an individual subsystem, considering neighboring nodes' angle deviations as decoupling variables. The dependency graph of the decomposition can be seen in Figure 1.12.

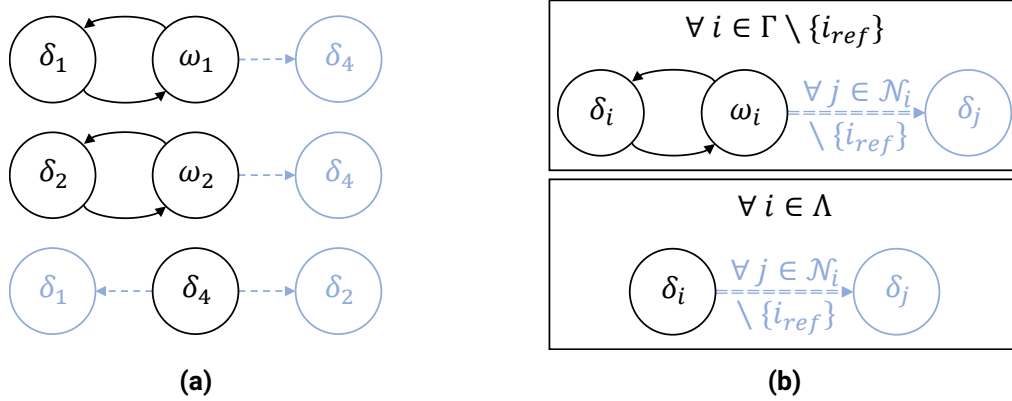


Figure 1.12: Dependency graph for the decomposition of the four-node- (a), and the arbitrary case (b). Decomposition variables taken as disturbance inputs are denoted by light color.

Although through such a decomposition the analyzed systems' state space dimension could technically be reduced to 2 and 1 for generator-, and load nodes respectively, the reduced subsystems are still interdependent on each other through the decomposition variables. Indeed, the advantages of decomposition is less obvious until it comes to set-based analysis introduced in Section 1.3. Instead of finding admissible set of Def. 6, and MRPI set of Def. 7 for the original, high-dimensional system (that would not be computationally plausible for large systems), lower dimensional \mathcal{A} and \mathcal{M} can be found for each decoupled subsystem.

Still, admissible, and MRPI sets depend on the decoupling variables (a node's neighbors' angular deviations), since they –even though treated as disturbance inputs– do affect the subsystems' dynamic behavior. Fortunately, we are considering an engineering application after all, and can rely on inequality constraints introduced in Section 1.1.1 that are constraints on loads' and generators' angular deviations (and possibly on generators' frequencies, although this project only considers the former). In other words, it is possible to define angular constraints $\delta_{\min,i}$ and $\delta_{\max,i}$ for each node as in (2.1), thus limiting the interval of values each decoupling variable can take, based on which the admissible-, and MRPI sets can be determined as described in Section 1.5.

One advantage of set-based decomposition is that admissible, and MRPI sets for the subsystems only depend on nodes directly connected to the node in question (the number of which in a real-life power grid is typically much smaller than in a full graph), easing computational complexity. Furthermore, applying the outlined approach to determine safe, potentially safe, and unsafe operating state areas (1.26) for each node, power grid operators need not analyze nodes whose post-fault state lies in the corresponding MRPI set, as those –per definition– are guaranteed to *ceteris paribus* stay inside the MRPI set, thus between angular inequality constraints as well.

As a consequence of aforementioned benefits, a single node's or connection's fault is less likely to trigger a constraint violation in a node further away, and so power sys-

tem supervision can concentrate their resources on topologically (and possibly also geographically) well-bounded areas following power system malfunction.

1.5 Determining Set Barriers for Power Grid Analysis

For a system to fulfill rotor angle stability (Section 1.1), it must be able to return to it's equilibrium point even if a single machine's state is changed between some finite constraints.

The barrier trajectory candidates of the admissible-, and MRPI set candidates are obtained by solving the initial value problem [13, S. 7], [15, S. 6]:

$$\begin{aligned} \dot{\mathbf{x}}_i(t, \mathbf{x}_i, \boldsymbol{\lambda}_i, \boldsymbol{\delta}_{\min}, \boldsymbol{\delta}_{\max}) &= \dot{\mathbf{x}}_{-,i} \cup \dot{\mathbf{x}}_{\sim,i} = \\ & \left[\begin{array}{c} \omega_i \\ \frac{\omega_R}{2H_i} \left(A_i - \frac{D_i}{\omega_R} \omega_i - \sum_{j=1, j \neq i} K_{ij} \cdot \sin(\delta_i - \delta_{\text{sat},ij} - \gamma_{ij}) \right) \end{array} \right] \\ \dot{\mathbf{x}}_i \Big|_{\mathbf{x}_i = [\delta_{\min,i} \ 0]} &= [0 \ 1]^T = \dot{\mathbf{x}}_{-,i}(\bar{t}_{-,i}) \\ \dot{\mathbf{x}}_i \Big|_{\mathbf{x}_i = [\delta_{\max,i} \ 0]} &= [0 \ -1]^T = \dot{\mathbf{x}}_{\sim,i}(\bar{t}_{\sim,i}) \end{aligned} \quad (1.29)$$

$$\begin{aligned} \dot{\boldsymbol{\lambda}}_i(t, \mathbf{x}_i, \boldsymbol{\lambda}_i, \boldsymbol{\delta}_{\min}, \boldsymbol{\delta}_{\max}) &= - \frac{\partial \dot{\mathbf{x}}_i(t, \mathbf{x}_i, \boldsymbol{\lambda}_i, \boldsymbol{\delta}_{\min}, \boldsymbol{\delta}_{\max})}{\partial \mathbf{x}_i} \boldsymbol{\lambda}_i = \dot{\boldsymbol{\lambda}}_{-,i} \cup \dot{\boldsymbol{\lambda}}_{\sim,i} = \\ & \left[\begin{array}{c} \lambda_{2,i} \frac{\omega_R}{2H_i} \sum_{j=1, j \neq i} K_{ij} \cdot \cos(\delta_i - \delta_{\text{sat},ij} - \gamma_{ij}) \\ -\lambda_{1,i} + \lambda_{2,i} \frac{D_i}{2H_i} \end{array} \right] \\ \boldsymbol{\lambda}_i \Big|_{\mathbf{x}_i = [\delta_{\min,i} \ 0]} &= [-1 \ 0]^T = \boldsymbol{\lambda}_{-,i}(\bar{t}_{-,i}) \\ \boldsymbol{\lambda}_i \Big|_{\mathbf{x}_i = [\delta_{\max,i} \ 0]} &= [1 \ 0]^T = \boldsymbol{\lambda}_{\sim,i}(\bar{t}_{\sim,i}) \end{aligned} \quad (1.30)$$

where

- $\mathbf{x}_i(t)$ is the i th machine barrier candidate trajectory consisting of the candidate trajectories $\mathbf{x}_{\leftarrow,i}(t)$, and $\mathbf{x}_{\rightarrow,i}(t)$ initiating (going backwards in time) from the lower-, and upper angular constraints respectively, and
- $\boldsymbol{\lambda}_i \neq \mathbf{0}$ is the nonzero solution to the adjoint equation consisting of the solutions to the lower-, and upper adjoint evolutions $\boldsymbol{\lambda}_{\leftarrow,i}(t)$, and $\boldsymbol{\lambda}_{\rightarrow,i}(t)$ respectively.

The barrier trajectory candidates intersect the angular constraint tangentially at some points in time $\bar{t}_{\leftarrow,i}$ and $\bar{t}_{\rightarrow,i}$. Thus, points $[\delta_{\min,i} \ 0]$ and $[\delta_{\max,i} \ 0]$ are also called the points of ultimate tangentiality.

The adjoint vector is at all times perpendicular to the barrier candidate [3, Eq. 6], and with that—as the conditions in (1.30) also suggest—the adjoint vectors are perpendicular to the angular constraints at the points of ultimate tangentiality.

Furthermore, $\delta_{\text{sat},ij}$ denotes the saturation function as described in [3, Eq. 10]:

$$\begin{aligned} \delta_{\text{sat},ij}(\delta_i, \lambda_{2,i}, \delta_{\min,j}, \delta_{\max,j}) &= \\ &= \begin{cases} \min(\delta_{\max,j}, \max(\delta_{\min,j}, \delta_i - \frac{\pi}{2} \text{sign}(\lambda_{2,i}))) & \text{for set } \mathcal{A} \\ \min(\delta_{\max,j}, \max(\delta_{\min,j}, \delta_i + \frac{\pi}{2} \text{sign}(\lambda_{2,i}))) & \text{for set } \mathcal{M} \end{cases} \end{aligned} \quad (1.31)$$

Let us combine the system dynamic \mathbf{x} and the adjoint equation $\boldsymbol{\lambda}$ into a vector \mathbf{c} :

$$\mathbf{c}(\mathbf{x}, \boldsymbol{\lambda}) = \begin{bmatrix} \mathbf{x} \\ \boldsymbol{\lambda} \end{bmatrix} \quad (1.32)$$

Then, the differential equation describing the barrier trajectories can be expressed as

$$\dot{\mathbf{c}} = \begin{bmatrix} \dot{\mathbf{x}} \\ \dot{\boldsymbol{\lambda}} \end{bmatrix} = \dot{\mathbf{c}}(\mathbf{c}, \boldsymbol{\delta}_{\min}, \boldsymbol{\delta}_{\max}) \quad (1.33)$$

$$\dot{\mathbf{c}}_i \Big|_{t=\bar{t}_{\leftarrow,i}} = [0 \ 1 \ -1 \ 0]^T \quad \forall i \in \{1 \dots n\} \setminus \{i_{\text{ref}}\} \quad (1.34)$$

$$\dot{\mathbf{c}}_i \Big|_{t=\bar{t}_{\rightarrow,i}} = [0 \ -1 \ 1 \ 0]^T \quad \forall i \in \{1 \dots n\} \setminus \{i_{\text{ref}}\} \quad (1.35)$$

that is, a function of each constraint in the whole system.

SET-VALIDITY ANALYSIS OF BARRIER TRAJECTORIES FOR ADMISSIBLE AND ROBUST INVARIANT SETS IN POWER SYSTEMS

2

Initial preliminary work in preparation to the topic of set-based transient stability analysis of power systems began with reproducing the example from [3, S. 5.1] on paper. As soon as a point was reached at which admissible-, and MRPI barrier candidates could be plotted, it was rather inevitable to come across the inconvenience of finding angular constraints that build valid sets for each machine in a power system model, and how this often involves meticulously adjusting angular constraints until such a set is found.

Our ultimate task was thus chosen as methodically finding angular constraints $\delta_{\min,i}$ and $\delta_{\max,i}$ for every generator besides the reference node so that aforementioned MRPI sets exist, given that

$$\delta_{\min,i} \leq \delta_i \leq \delta_{\max,i} \quad (2.1)$$

holds for all machines. Formulated otherwise, the goal setup was to find a solution $\boldsymbol{\delta}_{sol} = [\boldsymbol{\delta}_{\min} \quad \boldsymbol{\delta}_{\max}]^T$ for (1.33) subject to (1.34) and (1.35) resulting in valid trajectories for the describing the boundary of the admissible set and MRPI for each synchronous machine. The validity of these trajectories is discussed in Section 2.1.

2.1 Validity of MRPI Sets

In practice, the admissible-, and MRPI set barrier candidate trajectories are obtained by first fixing endpoints thereof in accordance with the criterion in (1.29) and (1.30), then performing numeric backwards integration of (1.33).

A valid MRPI set is one that fulfills the coherence criteria. For an MRPI set to be considered coherent, its boundaries must be defined by

- one or both of the angular constraint boundaries $\delta_i = \delta_{\min,i}$ and/or $\delta_i = \delta_{\max,i}$, and
- the barrier trajectory \mathbf{x}_i defined in (1.29) that intersect one or both of the angular constraint boundaries, and along which it holds that the adjoint vector is always directed towards out of the set in the interval between the two constraint barriers.

Please note that from this point on, the machine index will generally be omitted for the sake of simplicity. Thus, when the reader encounters notations such as δ , δ_{\min} , δ_{\max} , ω , \mathbf{x} , $\boldsymbol{\lambda}$, D , H , \dots , they should consider these as variables related to the i th machine: δ_i , $\delta_{\min,i}$, $\delta_{\max,i}$, ω_i , \mathbf{x}_i , $\boldsymbol{\lambda}_i$, D_i , H_i , etc.

In case of our interconnected second order oscillators (i.e. generators, as discussed in Section 1.2), two topologically distinct variants of a valid MRPI set may exist, as shown in Figure 2.1.

- On one hand, a valid MRPI set may look similar to that in Figure 2.1(a), both the lower, and upper MRPI barriers intersecting the opposite angular constraint. In this case, the MRPI set's boundary is defined by both barriers and both angular constraint boundaries. This will be referenced to as a **type A** MRPI set later in this work.
- On the other hand, a valid MRPI set may look like that in Figure 2.1(b), whose boundary is defined by one angular constraint boundary, as well as by one MRPI barrier intersecting said angular constraint boundary twice. This will be referenced to as a **type B** MRPI set later in this work.

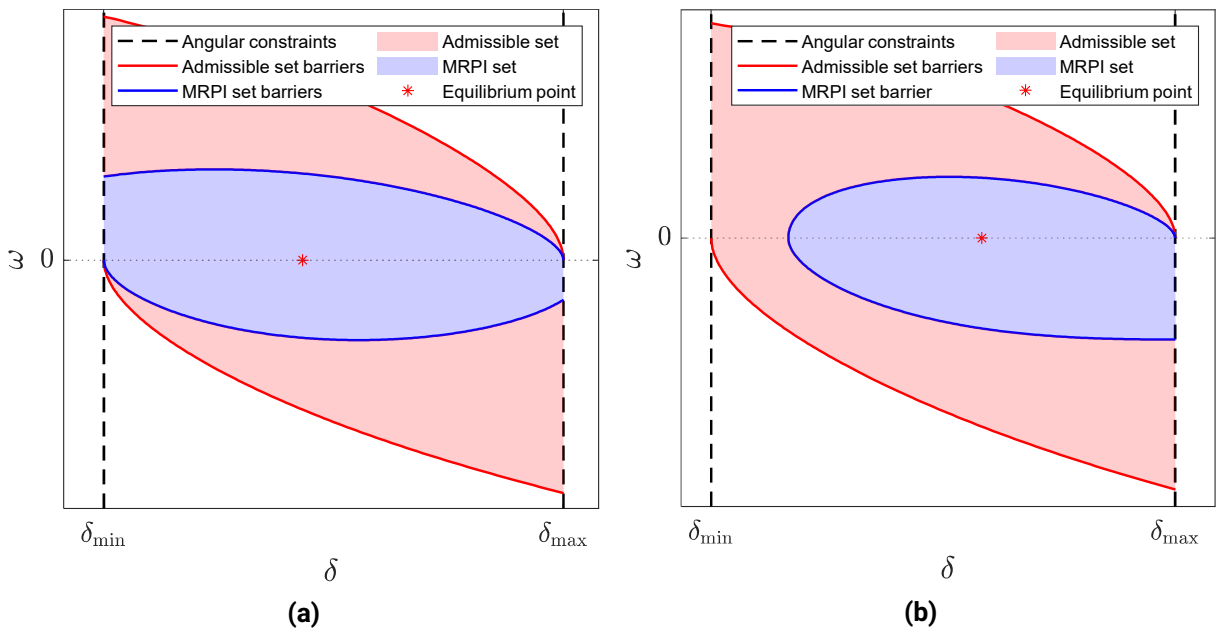


Figure 2.1: Examples of valid MRPI sets. (a): Type A. (b): Type B.

However, not all barrier candidates build a valid MRPI set, due to not fulfilling the criteria of coherence. Barrier candidates leading to an incoherent MRPI set may resemble those in Figure 2.2(a). Said incoherence can be attributed to two phenomena that are described in subsequent subsections.

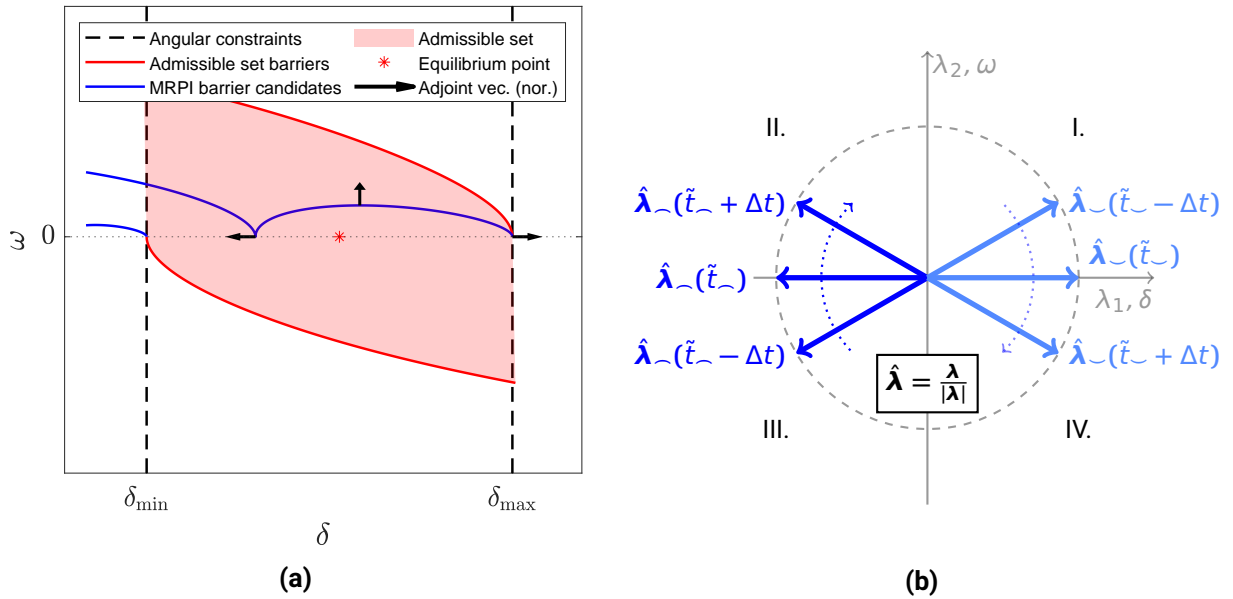


Figure 2.2: Evolution of the adjoint vector around the jumping point. (a): Phase diagram of a generator, displaying a valid admissible set, and MRPI barrier candidates that do not build a valid MRPI set. The upper barrier candidate represents the jumping phenomenon, while the lower barrier candidate represents constraint violation. (b): Direction change of the MRPI barrier candidates' adjoint vectors around the jumping point. Darker shades of blue represent the upper barrier candidate's adjoint vectors, while lighter blues refer to those of the lower barrier candidate. Roman numerals represent quadrants of the state plane.

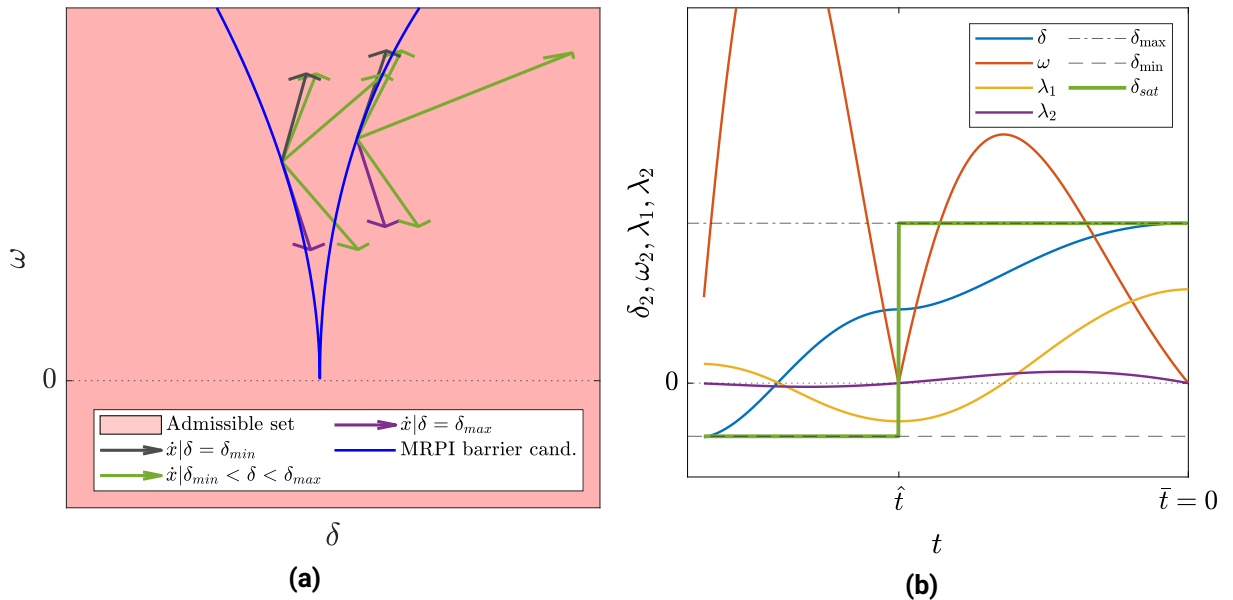


Figure 2.3: Diagrams of the jumping phenomenon. (a): A magnified section of an upper barrier candidate around the jumping point, showing state derivatives before- and after the jump. (b): Time domain plots for the MRPI barrier candidate, a section of which is shown in (a).

2.1.1 Constraint Violation

The barrier candidate tangentially intersecting the lower angular constraint boundary $\delta = \delta_{\min}$ (further referred to as the lower barrier candidate) in Figure 2.2(a) is not contained in \mathcal{A} , because [3, Proposition 1] is not fulfilled. This proposition states, that MRPI sets with boundaries \mathbf{x}_\leftarrow and/or \mathbf{x}_\rightarrow may exist if and only if $\dot{\mathbf{x}}_{\leftarrow,2}(\bar{t}_\leftarrow) = \dot{\omega}_\leftarrow(\bar{t}_\leftarrow) > 0$ and/or $\dot{\mathbf{x}}_{\rightarrow,2}(\bar{t}_\rightarrow) = \dot{\omega}_\rightarrow(\bar{t}_\rightarrow) < 0$ holds. Applying this along with $\omega = 0$ to (1.11) brings the conditions

$$A_i - \sum_{j \in \mathcal{N}_i} K_{ij} \cdot \sin(\delta_{\min,i} - \delta_j - \gamma_{ij}) > 0 \quad (2.2)$$

$$A_i - \sum_{j \in \mathcal{N}_i} K_{ij} \cdot \sin(\delta_{\max,i} - \delta_j - \gamma_{ij}) < 0 \quad (2.3)$$

Failing to fulfill above conditions, the barrier candidate trajectory will leave the constrained state space evolving backwards in time from the point of ultimate tangentiality. The lower MRPI barrier candidate in Figure 2.2(a) serves as an example of this phenomenon.

2.1.2 Jumping Phenomenon

The barrier candidate tangentially intersecting the upper angular constraint boundary $\delta = \delta_{\max}$ (further referred to as the upper barrier candidate) in Figure 2.2(a) is although contained in \mathcal{A} between the angular constraints, however, this trajectory does not constitute a valid MRPI barrier due to the so-called *jumping phenomenon* also shown enlarged in Figure 2.3(a). The jump is due to the signum function in (1.31), and can be characterized as follows

1. Let $\tilde{t} = \tilde{t}_\leftarrow$ denote the point in time at which the upper barrier candidate intersects the $\omega = 0$ axis. Running backwards in time starting from $\mathbf{x}_\leftarrow(\tilde{t}_\leftarrow) = [\delta_{\max} \ 0]$, as \mathbf{x}_\leftarrow approaches the jumping point $\mathbf{x}_\leftarrow(\tilde{t}_\leftarrow < \tilde{t}_\leftarrow)$, the adjoint vector $\boldsymbol{\lambda}_\leftarrow$ remains perpendicular to the barrier candidate at all times [3, Eq. 6]

$$\dot{\mathbf{x}}_\leftarrow(t) \boldsymbol{\lambda}_\leftarrow(t) = 0 \quad \forall t < \tilde{t} \quad (2.4)$$

and is always pointing outside of the proposed MRPI set as shown in Figure 2.2(a).

2. Every trajectory (including the barrier candidate trajectories) may only ever intersect the $\omega = 0$ axis perpendicularly due to $\dot{\delta} = \omega$ as in (1.11). This means, that when $\omega(\tilde{t}) = 0$, then $\dot{\mathbf{x}}(\tilde{t}) = [0 \ \dot{\omega}(\tilde{t})]^T$. This implies, in accordance with (2.4), that $\dot{\omega}(\tilde{t}) \lambda_2(\tilde{t}) = 0$. Since (going backwards in time) ω first decreases, then, without a sign change, increases again (i.e. changes direction as it touches the horizontal axis of the phase diagram), $\dot{\omega}$ must change sign just as ω becomes 0.
3. However, except for the signum function in (1.31), $\dot{\omega}$ is described in (1.29) through continuous functions. Thus, a sudden sign change can solely be attributed to the

saturation function undergoing a sudden value change due to λ_2 changing sign. That is, $\lambda_2(\tilde{t})$ must be 0.

4. The adjoint vector $\boldsymbol{\lambda}(t)$ is nonzero, and so because $\lambda_2(\tilde{t}) = 0$, it must be that $\lambda_1(\tilde{t}) \neq 0$.
5. From (1.30), $\dot{\lambda}_2 = -\lambda_1 + \lambda_2 \frac{D}{2H}$, which, due to point 3, simplifies to $\dot{\lambda}_2(\tilde{t}) = -\lambda_1(\tilde{t})$.
6. Due to points 4 and 5, $\dot{\lambda}_2(\tilde{t}) \neq 0$.
7. According to (1.30), $\dot{\lambda}_2$ is continuous, thus for some infinitesimal Δt , $\dot{\lambda}_2(\tilde{t} - \Delta t) \approx \dot{\lambda}_2(\tilde{t}) \approx \dot{\lambda}_2(\tilde{t} + \Delta t) \neq 0$. In other words $\dot{\lambda}_2$ does not undergo a sign change as the barrier candidate trajectory intersects the $\omega = 0$ axis.
8. As a consequence of points 5 and 7, $\lambda_1(\tilde{t} - \Delta t) \approx \lambda_1(\tilde{t}) \approx \lambda_1(\tilde{t} + \Delta t) \neq 0$. Thus, neither does λ_1 undergo a sign change as the barrier candidate trajectory intersects the $\omega = 0$ axis.

This means, that since the direction of $\lambda_{1,i}$ does not change, but that of $\lambda_{2,i}$ does change between before and after the jump, $\boldsymbol{\lambda}(\tilde{t} - \Delta t)$ must be in the adjacent quadrant to $\boldsymbol{\lambda}(\tilde{t} + \Delta t)$. In case of the upper barrier candidate in Figure 2.2(a), the adjoint vectors are in the II. quadrant before the jump (going backwards in time), and in the III. quadrant thereafter. How the $\boldsymbol{\lambda}$ undergoes a quadrant change is shown in Figure 2.2(b).

However, since the adjoint vectors should point outwards of the proposed MRPI set (see Figure 2.4), and the MRPI set must be coherent, this leads to a contradiction.

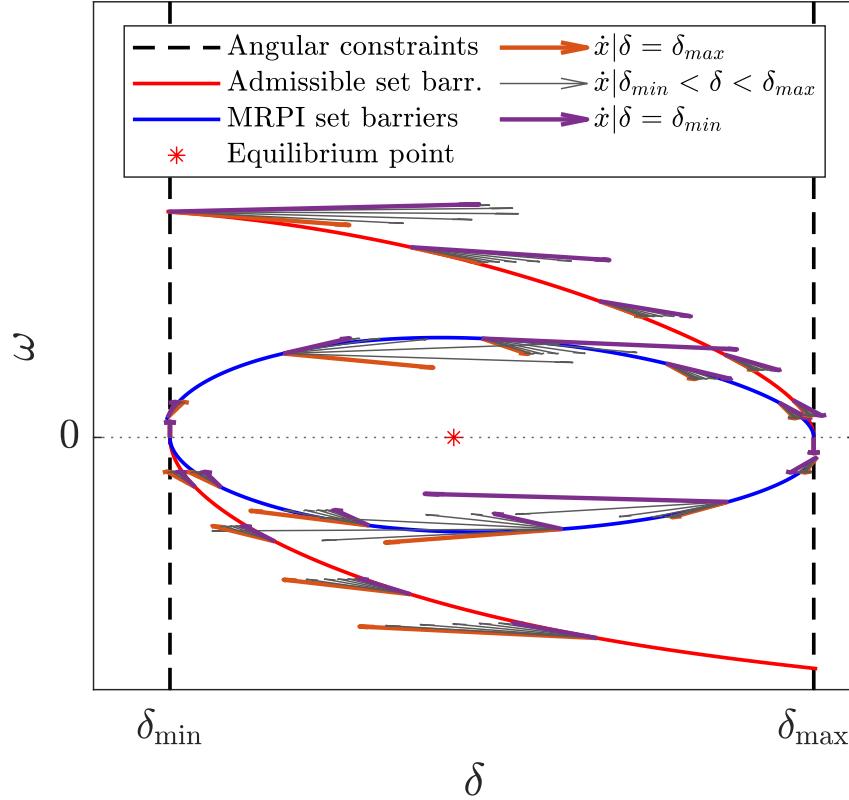


Figure 2.4: Vectogram along valid set barriers for saturated-, as well as unsaturated cases. Notice how on the MRPI set barriers, all the state derivative vectors point towards the inside, except for one vector in each point, which is tangential to the barrier trajectory. The same is true for the admissible set barriers, except for that here all state derivative vectors point towards outside of the admissible set, except for the one in each point that is tangential to the admissible set barrier.

Indeed, in Figure 2.3(a), some state derivative vectors are shown along the MRPI barrier candidate before- and after the jump (for δ_{\min} , δ_{\max} , and further interim δ values). On the right hand side, these vectors all point inwards of the barrier candidate (except for one, as for exactly one δ value, said state derivative vector is tangential to the barrier candidate). This makes intuitive sense, as the very definition of an invariant set in Def. 3 is that for any starting state inside it, the state evolution will stay inside the invariant set for all future points in time.

On the left hand side of Figure 2.3(a), state derivatives point towards the opposite side of the barrier candidate, which does not facilitate a coherent MRPI set.

As for where barrier jumping may or may not occur, Figure 2.5 is intended to serve as an overview. Since $\delta_{\text{sat}}(\mathbf{x}, \boldsymbol{\lambda}, \delta_{\min}, \delta_{\max}) : \mathbb{R}^2 \times \mathbb{R}^2 \times \mathbb{R} \times \mathbb{R} \rightarrow [\delta_{\min}, \delta_{\max}]$, if

$$\left(\dot{\omega} \Big|_{\omega=0, \delta_{\text{sat}}=\delta_{\min}} \right) \cdot \left(\dot{\omega} \Big|_{\omega=0, \delta_{\text{sat}}=\delta_{\max}} \right) > 0 \quad (2.5)$$

then $\dot{\omega}$ cannot change sign as the MRPI barrier candidate approaches the $\omega = 0$ axis, and so no jumping will occur. A statement about whether a jump occurs if (2.5) is not fulfilled, is up for further mathematical analysis, as it might depend on what value δ_{sat} takes as the trajectory crosses $\omega = 0$.

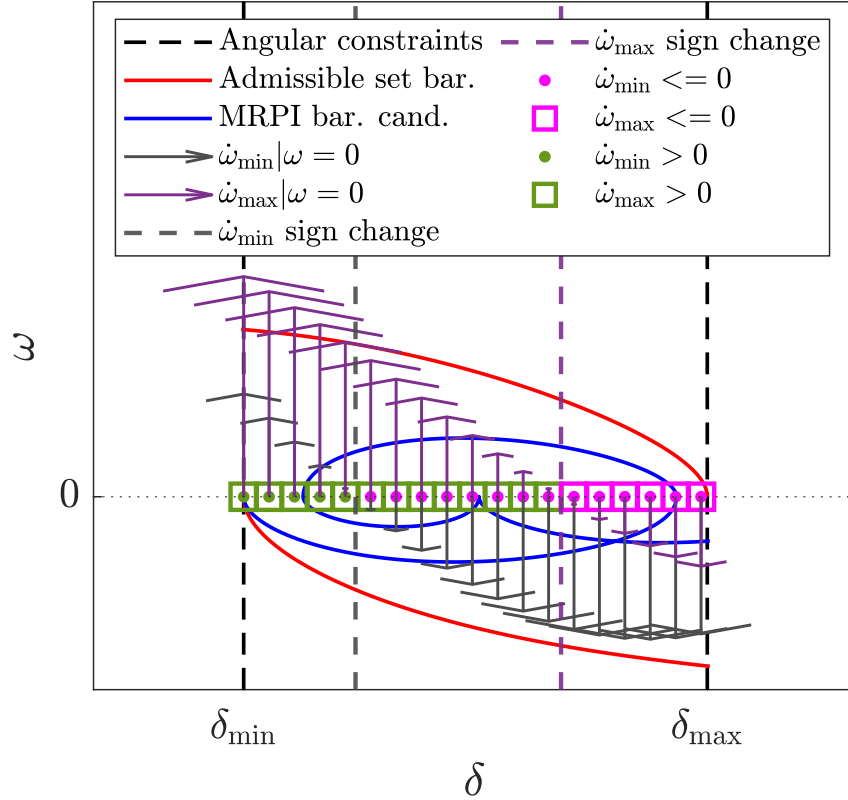


Figure 2.5: Jumping conditions along the $\omega = 0$ axis.

Generally all considerations regarding set coherence, constraint violation, and the jumping phenomenon hold not only for MRPI set barrier candidates, but admissible set candidates as well. However, because $\mathcal{M} \subset \mathcal{A}$ given $\mathcal{A} \neq \emptyset$, the validity of an MRPI set implies the existence of a valid admissible set. Thus, whether MRPI barrier candidates build a coherent MRPI set is the narrower question –as Figure 2.2(a) also illustrates– worth examining.

2.2 Research Framework Setup

Subsequent efforts were focused towards laying out a method for finding valid MRPI sets. To better facilitate experimenting, barrier candidate plotting in MATLAB was implemented in a rather parameterized manner, so that arbitrary model network structures can be loaded either by supplying model parameters directly, or with the help of the MATPOWER library, by preparing a case file with the electrical properties of the physical power network, and letting MATPOWER generate the model [42].

Utilizing the latter method, further experimentation with the 9-bus-system from [12] –as provided through [32]– took place. During our experiments, machine 1 has always been assumed to be the reference machine for which $\omega_1 \equiv 0$ holds, since –as it is also shown in Figure 2.6– it has the highest inertia constant of all three machines.

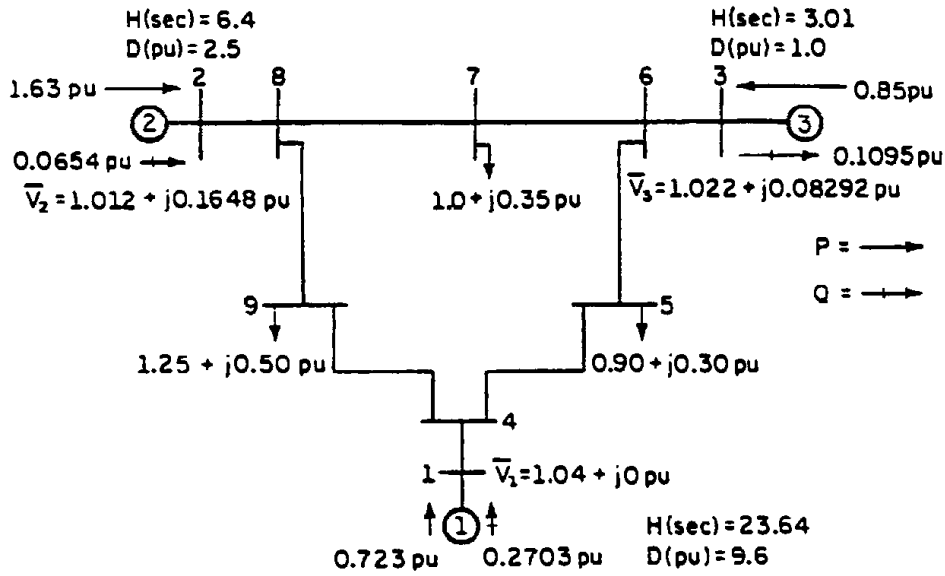


Figure 2.6: The three-machine, nine-bus test system. During experimentation, machine 1 served as the infinite bus throughout. From [12, Fig. 4.3.1].

Furthermore, the nine-bus system has not been examined as-is, but its effective network model was considered. The effective network model (EN model for short) was initially proposed by [29], and is also referred to as the network-reduction model or network-reduced model. Although a detailed discussion of this model is omitted from this work, a brief introduction is nonetheless necessary. The essential consideration of the EN model is that the nature of coupling between a pair of generators connected to the same power grid is primarily determined by the structure of the transmission lines and loads in between the generator nodes [31, S. 4.1], while the dynamical interaction between said generators is described by applying the classical model's power-angle equation (1.5) for both machines. Effective network representation is concerned with grasping the effect of aforementioned intermediate network structure on the dynamic interaction of each pair of generators through a single term that depends only on the generators' state variables. In practice, the effective network model of an arbitrary oscillatory network of loads and generators (first- and second order oscillators) is formed by applying a network reduction method (called Kron-reduction) to the original system, resulting in a fully connected network of only the generators of the original system, with load nodes (first order oscillators) completely eliminated.

Besides plotting phase diagrams as in Figure 2.1 and barrier candidates, further graphics have been constructed to improve understanding of set-based power-system dynamics. These include vector meshes of the state derivative vectors as in Figure 2.7, vectograms along barrier (candidate) trajectories as in Figure 2.4, time domain plots as in Figure 2.3(b), as well as plots of jumping conditions as in Figure 2.5.

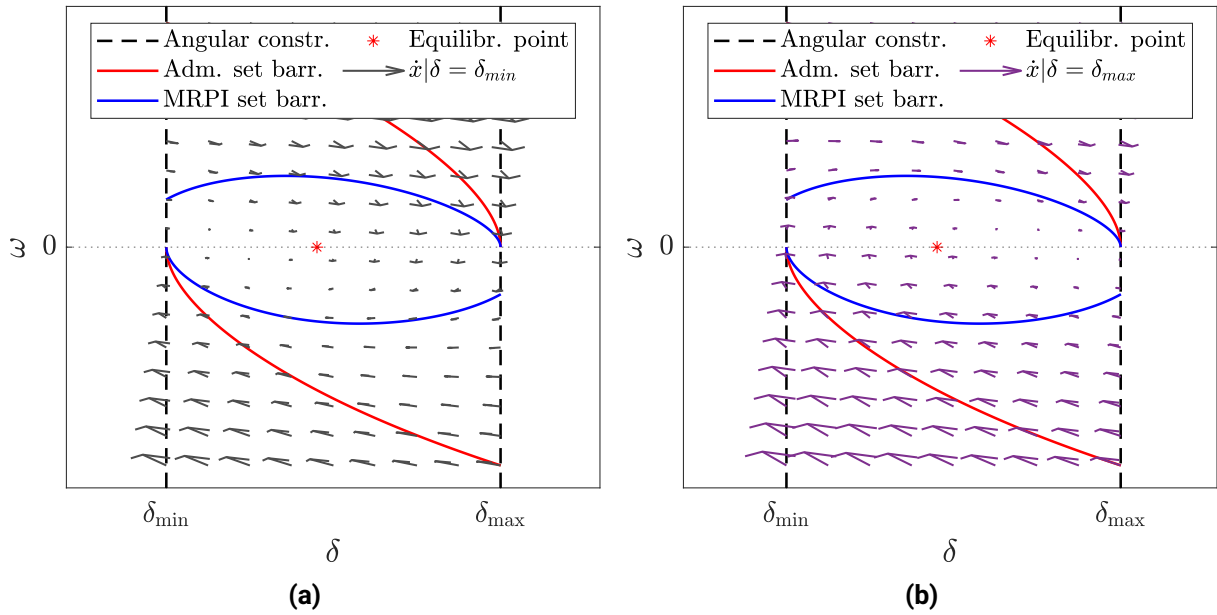


Figure 2.7: Quiver plots of the saturated state derivatives.

2.3 Interactive Slider

In pursuing intuition of how angular constraints of valid MRPI sets could programmatically be found, a panel of four sliders in MATLAB was implemented, where the slider values corresponded to the lower-, and upper angular constraints of the two non-reference machines (machines 2 and 3) in the nine-bus system's effective network model representation. Figure 2.8 shows a screen grab of aforementioned slider in use.

As for the sliders, the underlying script was written in such a way, that desired graph types (out of the aforementioned options) can be input as parameters, and so once it is run each adjustment made to a slider will cause the power system model to be re-evaluated, and graphics to be updated accordingly.

Through further modification to the source code, a functionality was too implemented, in which start, and end values of angular constraints can be input as parameters along with a desired angle step size vector (that is, an angular step size for each minimal/maximal angular constraint for every non-reference machine), resulting in a sequence of plot images that can easily be converted to a video using external tools.

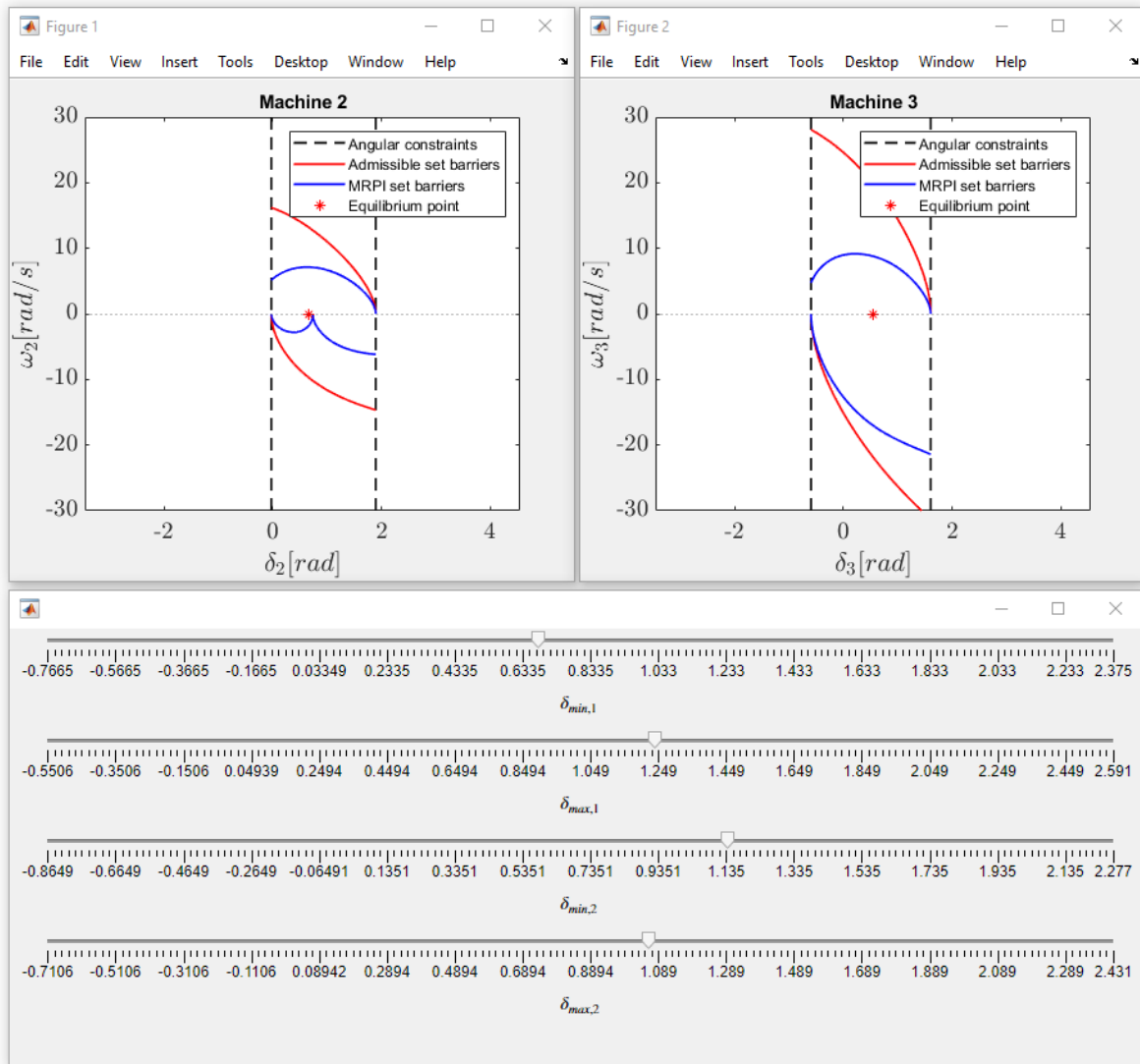


Figure 2.8: Sliders with angular constraint values.

Through experimentation, soon two observations were made:

- At least for this nine-bus system it is very much possible to find valid set pairs by hand (through setting the sliders), even though modifying any slider value (any constraint) has an effect on the whole network dynamics. After some experimentation one seemed to be able to improve the *skill* of finding valid sets by hand, starting with randomized initial values for angular constraints. However, this *skill* was of rather intuitive kind, thus supporting the idea that a neural network might be an option at tackling the task at hand.
- It seems that as one continuously modifies solely one constraint of a single machine in a given direction, then the phase diagram of the MRPI barrier candidates go through *phases* of well recognizable characteristics.

2.4 Observation on Barrier Phases

As a demonstration of the latter phenomenon, phase diagrams representative of aforementioned stages will now be illustrated. For this demonstration, only the admissible set barriers, and the upper MRPI barrier candidate will be shown (but –for better visibility– not the lower MRPI barrier candidate). Initially, the nine-bus system from before was simulated with such angular constraints that would lead to an initial upper MRPI barrier candidate as shown in Figure 2.9 for one of the machines. The initial difference of this observed machine’s angular constraints will be taken as 100%, and the upper angular constraint δ_{\max} will be increased in subsequent stages. All other constraints (of every machine in the network) will be left unchanged.

In the below discussion, *before*, *after*, *first*, and *last* will be used backwards in time for conveniency. That is, point $[\delta_{\max} \ 0]$ (the upper point of ultimate tangentiality) will be spoken of as if it would be the starting point of the upper MRPI barrier candidate, out of which the latter propagates, even though the opposite is true.

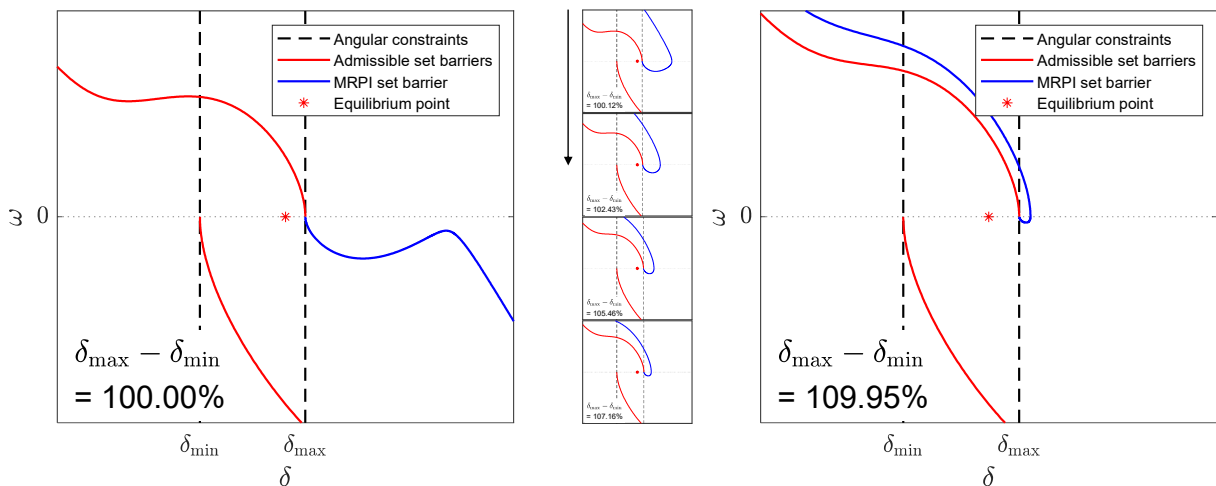


Figure 2.9: Stage 1 MRPI barrier phase.

Initially, the MRPI barrier candidate evolves in the undesirable direction as (2.3) is not yet fulfilled. This condition remains unfulfilled until the barrier candidate approaches the upper admissible barrier as shown in Figure 2.9.

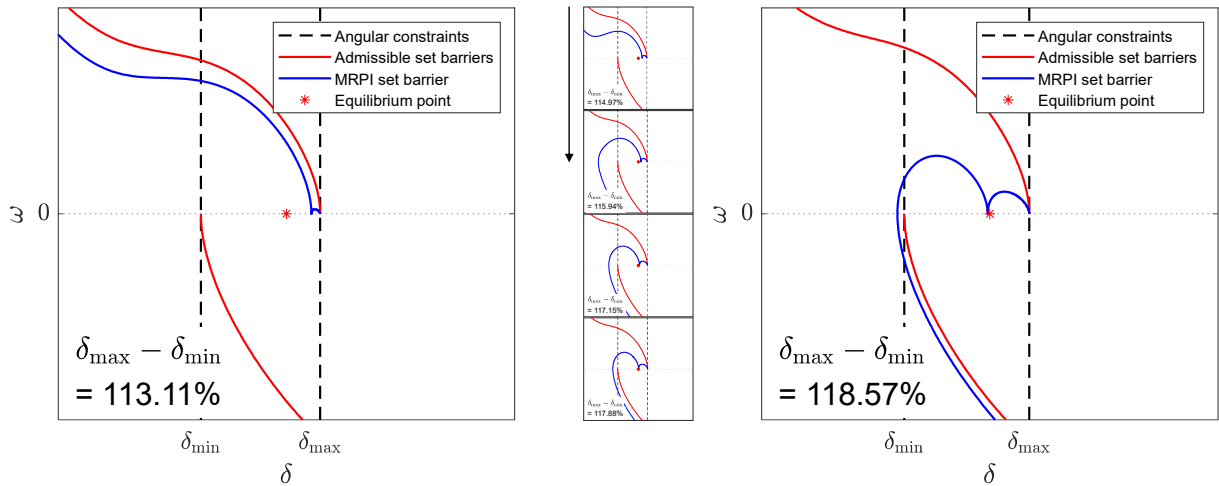


Figure 2.10: Stage 2 MRPI barrier phase.

As (2.3) gets fulfilled, the MRPI candidate continues to propagate between the angular constraints and inside the admissible set, making a jump –as described in Section 2.1– before intersecting the opposite angular constraint $\delta = \delta_{\min}$.

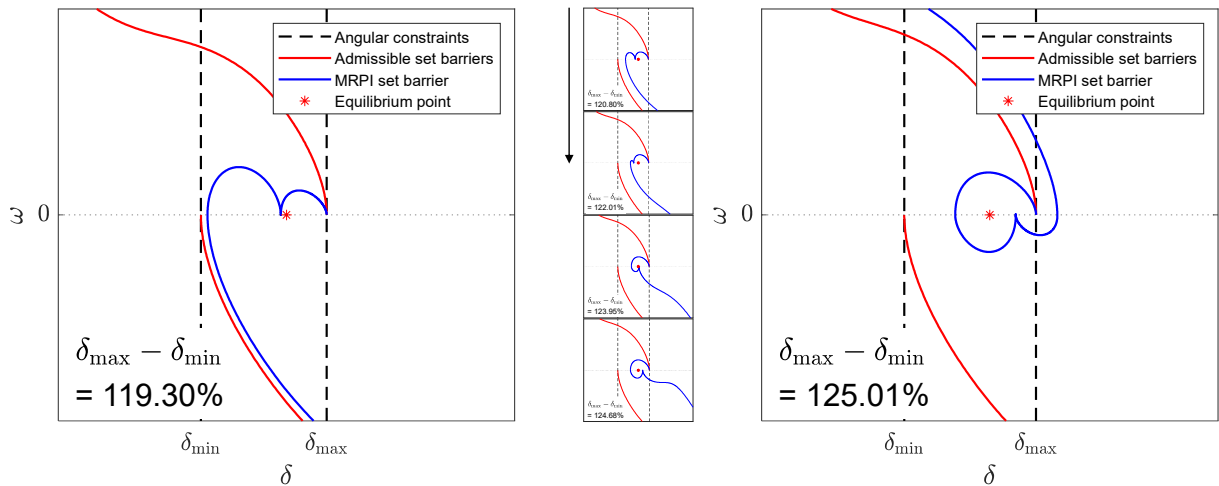


Figure 2.11: Stage 3 MRPI barrier phase.

The MRPI barrier candidate will eventually intersect the lower admissible barrier and the lower angular constraint exactly in the point of ultimate tangentiality. From here on, the upper MRPI set barrier will not intersect with the lower angular constraint before intersecting the upper angular constraint for the second time during its evolution. The jumping point will continue propagating towards the opposite constraint (towards left) until the jump *folds over* to the $\omega < 0$ side. That is, a δ_{\max} value will eventually be reached, at which the first time the MRPI barrier candidate reaches the $\omega = 0$ axis, it will pass through it, and a jump will occur from *below*.

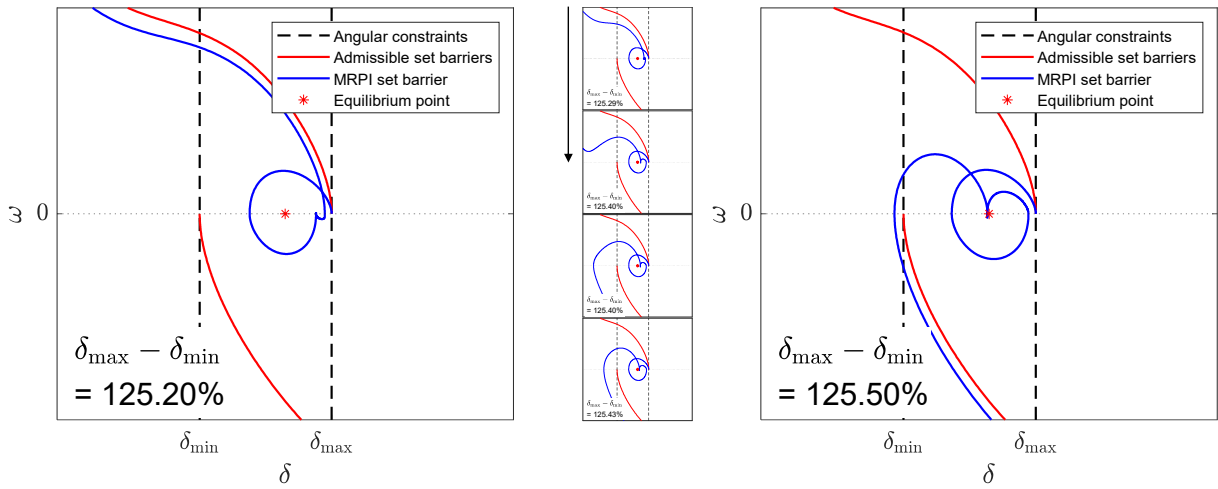


Figure 2.12: Stage 4 MRPI barrier phase.

Then, the barrier candidate's *tail* continues *rotating* in counterclockwise direction. The barrier candidate's jumping point will again *fold* over to the $\omega > 0$ side, as the candidate approaches the lower admissible set barrier.

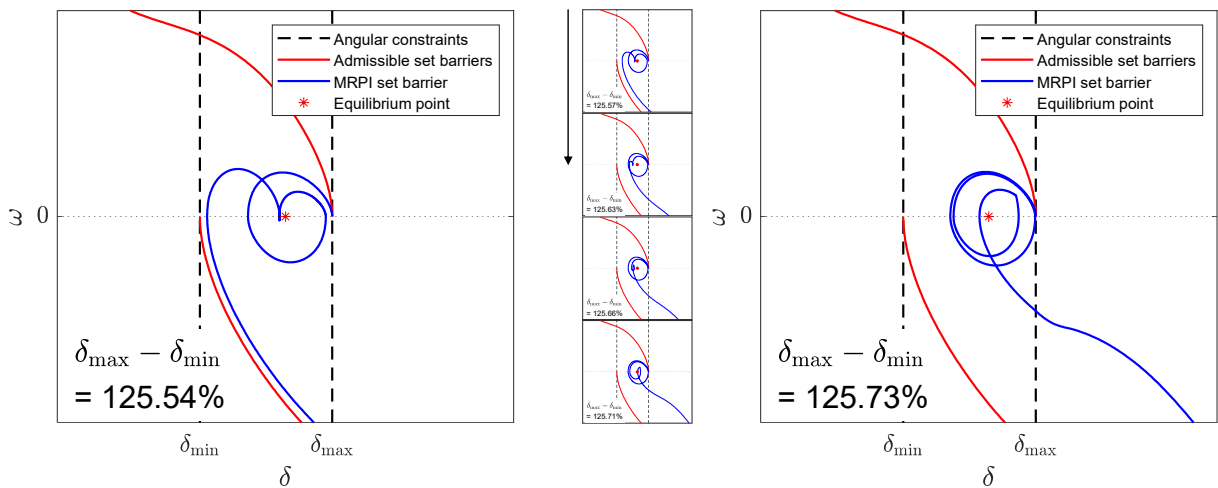


Figure 2.13: Stage 5 MRPI barrier phase.

As we pass the lower admissible set barrier for the second time, we start to see a pattern in which the MRPI barrier candidate's *tail* continues to evolve outwards, in a direction that is rotating anticlockwise as δ_{\max} increases, while the jumping point folding over again and again, with the jumping phenomenon happening after more and more crossings of the $\omega = 0$ axis. This pattern continues until the *tail's* rotation slows and finally changes direction.

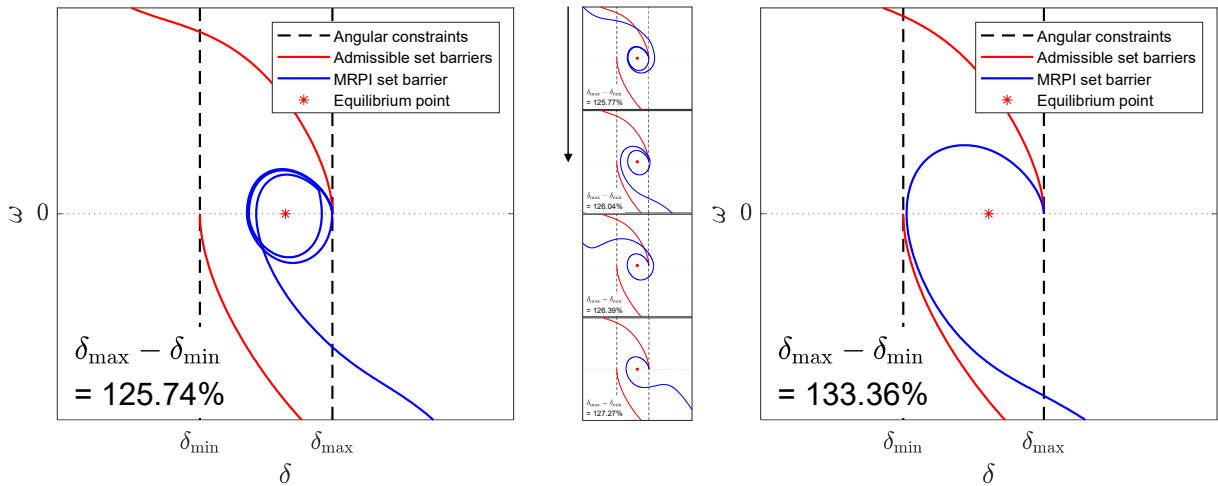


Figure 2.14: Stage 6 MRPI barrier phase.

After the direction change, the barrier candidate will continue *rotating* in the opposite (clockwise) direction much like as if the the MRPI barrier candidate trajectory would *unwind* from an imaginary *reel* whose axis goes through the equilibrium point and is perpendicular to the $\delta - \omega$ plane as can be observed in Figure 2.14. This continues until the MRPI barrier candidate intersects with the point of ultimate tangentiality of the opposite constraint, $[\delta_{min} 0]$ in this case. This is exactly the point from where the opposite barrier trajectory of the admissible set initiates (going backwards in time).

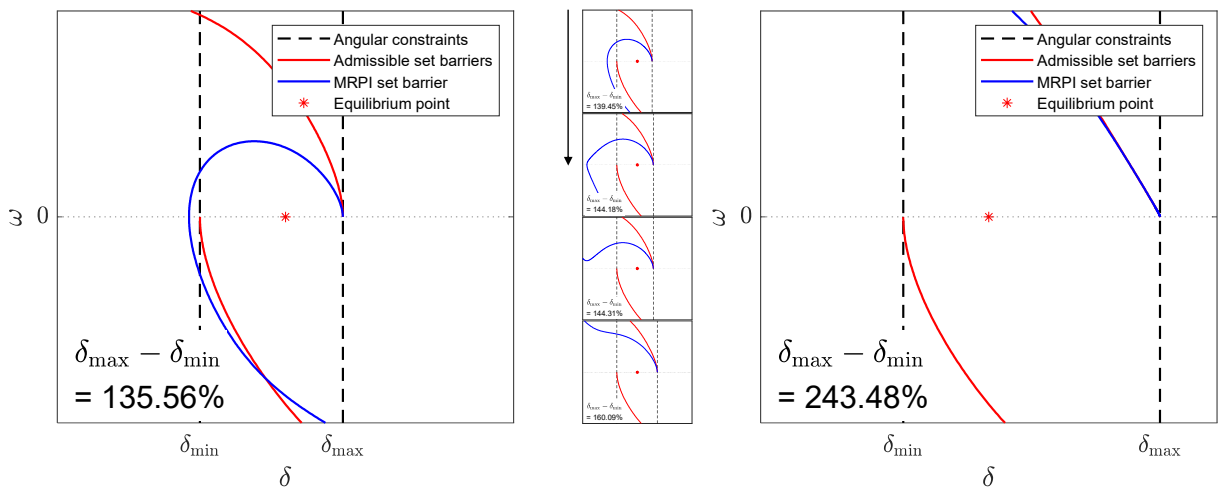


Figure 2.15: Stage 7 MRPI barrier phase.

From this point on, the MRPI barrier candidate propagates in an arch that crosses the opposite angular constraint at an ever higher $|\omega|$ value, as it approaches the same-side (in our case, the upper) admissible set barrier.

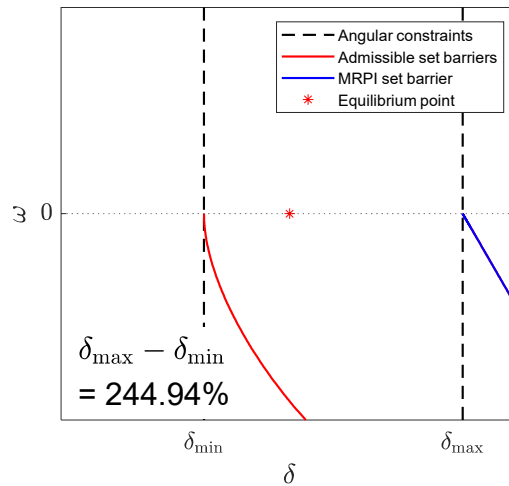


Figure 2.16: Stage 8 MRPI barrier phase.

Finally, as δ_{\max} further increases, (2.3) gets unfulfilled, resulting in both the upper MRPI- and admissible set barrier candidates propagating in the invalid direction, outside of the interval between the angular constraints as shown in Figure 2.16.

Table 2.1 overviews the evolution of the above discussed 8 stages of MRPI barrier candidate trajectories and their characteristics in each stage.

St.	Rot.	Start				End				$\Delta\Delta\delta$ [pp]
		$\Delta\delta$ [%]	Dev.	Q.	V.	$\Delta\delta$ [%]	Dev.	Q.	V.	
1	CCW	100,00	O	IV.	N	109,95	$O\bar{C}$	II.	N	9,95
2	CCW	113,11	\bar{J}	II.	N	118,57	$\bar{J}\bar{C}$	IV.	N	5,46
3	CCW	119,30	$\bar{J}\bar{C}$	IV.	N	125,01	$\bar{C}\bar{J}\bar{C}$	II.	N	5,71
4	CCW	125,20	$\bar{C}\bar{J}\bar{C}$	II.	N	125,50	$\bar{C}\bar{C}\bar{J}\bar{C}$	IV.	N	0,30
5	CCW	125,54	$\bar{C}\bar{C}\bar{J}\bar{C}$	IV.	N	125,73	$\bar{C}\bar{C}\bar{C}\bar{C}\bar{C}$	IV.	N	0,19
6	CW	125,74	$\bar{C}\bar{C}\bar{C}\bar{C}\bar{C}$	IV.	N	133,36	\bar{C}	IV.	Y	7,62
7	CW	135,56	B	IV.	Y	243,48	B	II.	Y	107,92
8	CW	244,94	O	IV.	N					

Table 2.1: Characteristics of MRPI barrier candidate trajectory phases. Abbreviations are as follows: **St.:** Stage; **Rot.:** Rotation (CW: Clockwise, CCW: Counter-Clockwise); **$\Delta\delta$:** The $\delta_{\max} - \delta_{\min}$ distance prevalent towards the start-, or end of the phase as a percentage of the initial distance; **Dev.:** Development of the barrier trajectory as going backwards in time (O : "Out", the barrier trajectory violates (2.2)-(2.3), J : Jumping in $\omega = 0$, C : Crossing the $\omega = 0$ axis, B : Boundary of the opposite angular constraint crossed). Underlines and overlines represent whether a jump or an axis intersection took place as the trajectory was approaching the $\omega = 0$ axis from the $\omega < 0$ half plane or not respectively as time progresses backwards; **Q.:** Quadrant of the state-plane towards which the barrier candidate evolves as going backwards in time; **V.:** Validity of the barrier candidate, as in whether it could constitute a barrier of a consistent MRPI set (N: No, Y: Yes); **$\Delta\Delta\delta$:** Change in $\Delta\delta$ between the start and end of the phase in percentage points.

So far this demonstration focused on an upper MRPI barrier candidate of a machine, and what happens as one increases the upper constraint's value of that same machine. However, experimental results suggest that the conjecture regarding barrier candidate stages can be further extended. Given that

1. a *single* machine's phase diagram is being observed, and
2. a *single* angular constraint value of either the same *or another* machine —and nothing else— is being altered in a given direction

then the phase diagram will go through the aforementioned stages in either *forward or backward* order, *if at all*.

Would the conjecture hold, it would have implications as follows. Let us assume, that a single constraint value (a slider) is, say, increased, and consequently a barrier candidate trajectory of a machine would change from stage 4 to stage 3. Then, resetting and

decreasing the same value instead would cause the barrier candidate to either remain in stage 4 or transition to stage 5, but never to transition to stage 3.

Furthermore, above observations seem to apply to both upper-, and lower barrier candidates; in the latter case each stage would look similar to that of the upper bound but mirrored to roughly the $\omega = -\delta$ line.

Of the aforementioned developmental stages, MRPI barrier candidates of stage 6 or 7 may possibly serve as a valid MRPI barrier candidate of the observed machine. In the former case, a single MRPI barrier as in Figure 2.1(b), and in the latter, two (an upper and lower) stage 7 MRPI barriers as in Figure 2.1(a).

Most importantly, would the conjecture and its aforementioned implications be true, it would further suggest, that a methodical search for valid MRPI sets would be possible by the means of gradual adjustment of the angular constraints.

2.5 Barrier phases and set validity

Table 2.1 shows that barrier stages 6 and 7 may constitute valid MRPI barrier candidates. It has been elaborated in the table's caption that validity in this sense refers to whether the barrier trajectory in question could constitute a barrier of a consistent MRPI set. The current section aims to discuss how statements about barrier phases translate to statements about MRPI set consistency. To facilitate further investigation, we are going to take a look at the one machine, one bus example from [3, 5.1], that embodies a most basic power network with a single generator connected to a single load as depicted in Figure 2.17.

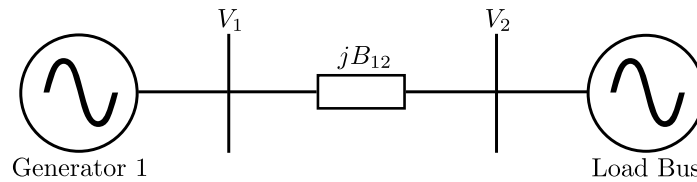


Figure 2.17: Topography of the one machine, one bus system. From [3, Fig. 2].

In describing the dynamics of the above system, the sole generator and load were considered as second-, and first order coupled oscillators respectively, described by the swing equation (1.6). Figure 2.18 depicts the phase diagrams of above system for unchanged system parameters except for growing $\delta_{\max,2} = -\delta_{\min,2}$ values between 0 and $\frac{\pi}{2}$.

Observing the lower MRPI barrier candidate, we see that although it gets further and further away from the lower admissible set barrier, it remains a phase 7 barrier candidate. Actually, according to the proposition in Section 2.4, what we see is the phase 7 MRPI barrier transition as in Figure 2.15, playing out in reverse (towards phase 6) as $\delta_{\max,2}$ grows.

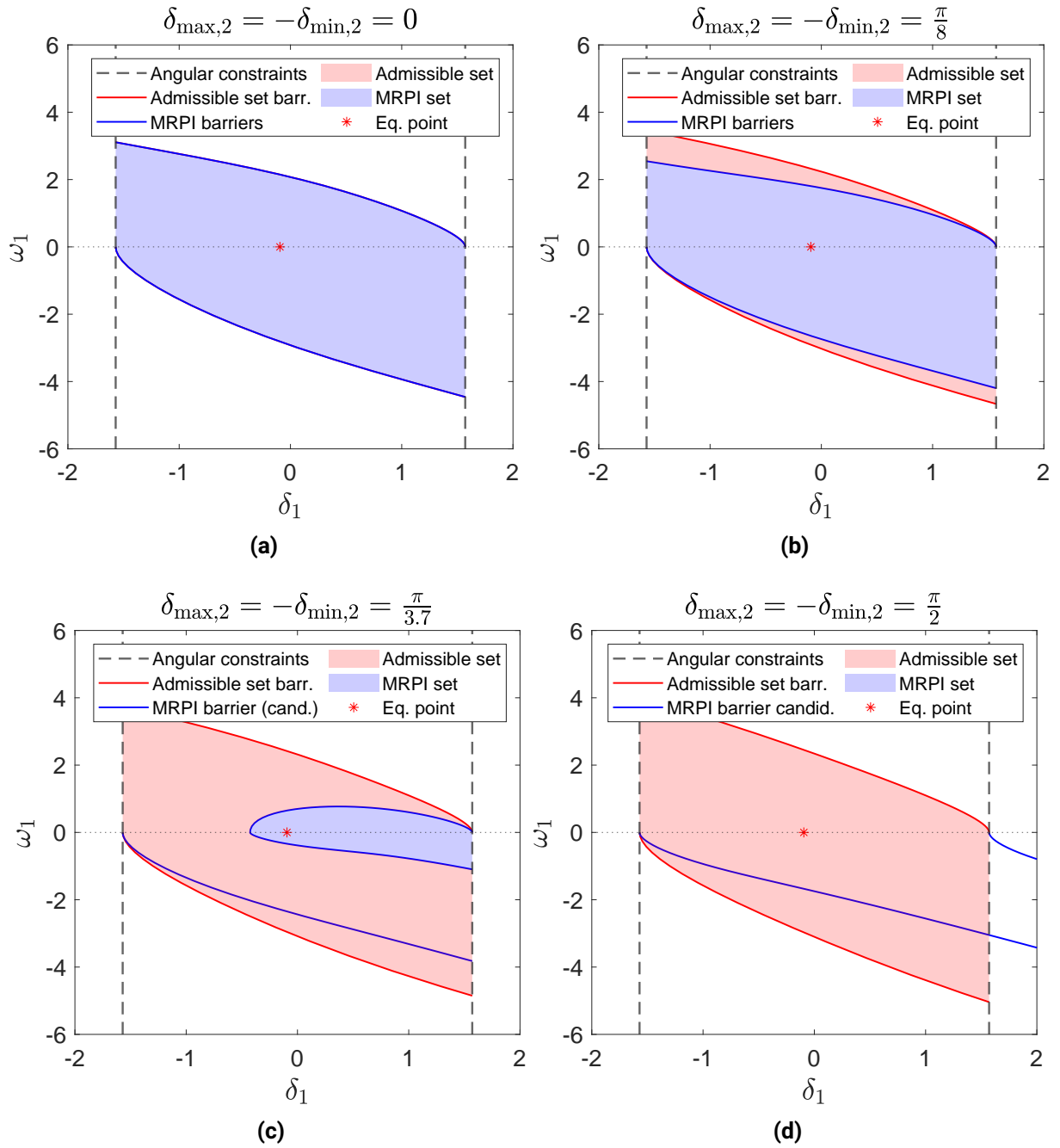


Figure 2.18: Barrier phases in the one machine one bus system from [3, S. 5.1], shown in Figure 2.17. Index 1 represents the sole generator node (modeled as a second order oscillator), and 2 the load node (modeled as a first order oscillator). (a): Both MRPI barriers are of phase 7 as in Figure 2.15. The MRPI and admissible sets coincide. (b): Both MRPI barriers are still of phase 7, but as δ_{\max} increases, the admissible set grows bigger, while the MRPI set shrinks. Nonetheless, the MRPI barriers still build a consistent type A MRPI set (see Figure 2.1). (c): The lower MRPI barrier is of phase 7, while the upper one is of stage 6, intersecting the upper angular constraint twice, building a type B MRPI set. (d): The lower angular constraint is of phase 7, and the upper one is of phase 8 as (2.3) does not get fulfilled. Note that this subfigure (unlike the other three) shows the barrier candidate evolutions before (going forward in time) they intersect with the upper angular constraint. The reasoning behind this exception is that this way the upper MRPI barrier candidate's evolution is visible.

Regarding the upper MRPI barrier candidate, subfigures (a) and (b) show the same phase 7 transition as with the lower MRPI barrier. Then, as $\delta_{\max,2}$ further grows, the upper MRPI barrier enters phase 6 in subfigure (c), eventually going through all the interim phases until reaching phase 1 in subfigure (d).

As for how these phase evolutions translate to statements about the consistency of the MRPI set, the following can be said:

1. Two phase 7 MRPI barrier candidates *will* build a consistent type A –as in Figure 2.1(a)– MRPI set for the observed machine.
2. A single phase 6 MRPI barrier candidate *may* build a consistent type B –as in Figure 2.1(b)– MRPI set if the barrier candidate does not undergo the jumping phenomenon, nor are loops in the barrier candidate’s evolution between the observed machine’s angular constraints.
3. Barrier candidates of phase 1-5 and 8 *do not* contribute towards building a consistent MRPI set.

2.6 Iterative approach towards finding consistent MRPI sets

Because of the connection between barrier phases and MRPI sets, it can be presumed that an iterative algorithm capable of finding consistent MRPI sets exists. To support this statement, an example considering the nine-bus system will be provided in this section. In it, the Effective Network model of the nine-bus system (see Figure 2.2) is considered as provided through [32], and the slider from Section 2.3 is utilized.

We choose arbitrary initial constraints, so that they are 1.6 rad away from the corresponding machines’ equilibrium points. This results in phase diagrams as shown in Figure 2.19.

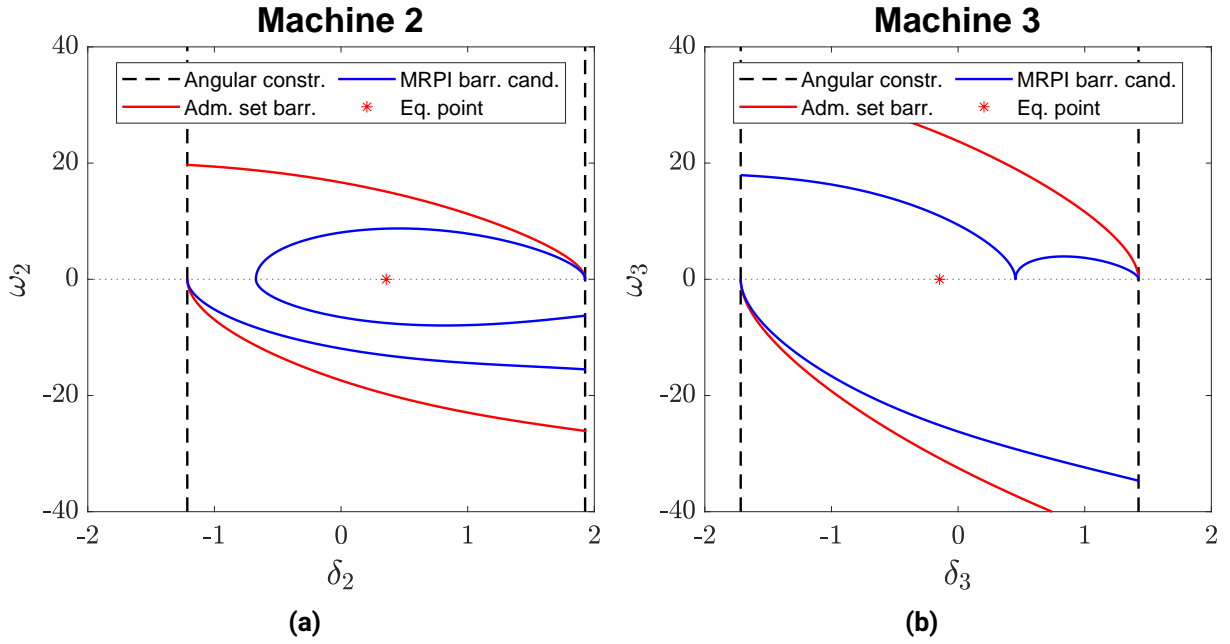


Figure 2.19: Phase diagrams of the two non-reference machines when angular constraints are $[\delta_{\min,2}, \delta_{\max,2}, \delta_{\min,3}, \delta_{\max,3}] = [\delta_{\text{eq},2}, \delta_{\text{eq},2}, \delta_{\text{eq},3}, \delta_{\text{eq},3}] + [-1.6, 1.6, -1.6, 1.6]$

Then, we consider the phase of each MRPI barrier candidate, while also examining, what effect a change in each angular constraint's value inflict on the barrier candidates. For our purposes, we will only note down angular constraints that have a *notable* effect on the barrier candidate in question. These are summarized in Table 2.2.

MRPI barrier candidate	2U	2L	3U	3L
Phase	6	7	2	7
Relevant angular constraint	$\delta_{\max,2} \rightarrow$ $\delta_{\max,3} \leftarrow$	$\delta_{\min,2} \leftarrow$	$\delta_{\max,2} \leftarrow$ $\delta_{\max,3} \rightarrow$	$\delta_{\min,3} \leftarrow$

Table 2.2: Initial phases of each MRPI barrier candidate, and angular constraints they are most affected by. Barrier candidates are denoted by the machine number, and "U" for the upper and "L" for the lower barrier candidate. Arrows mean that changing the angular constraint (slider) in that direction results in the barrier candidate in question to transition towards phase 8. For example, decreasing $\delta_{\max,2}$ and/or increasing $\delta_{\max,3}$ shifts the upper barrier candidate of machine 3 from phase 2 towards phase 3 (and the upper barrier candidate of machine 2 towards phase 5).

The upper barrier candidate of machine 2 builds a consistent type B MRPI set, however, the barrier candidates (of phases 2 and 7) of machine 3 do not result in a consistent MRPI set of any kind. Intuitively, one might try to shift the upper barrier candidate of machine 3 to phase 6 or 7. Looking at Table 2.2 we see that this can be done by decreasing $\delta_{\max,2}$ and increasing $\delta_{\max,3}$. Let us do so by the amount of 0.1 rad in both cases. The results are shown in Figure 2.20.

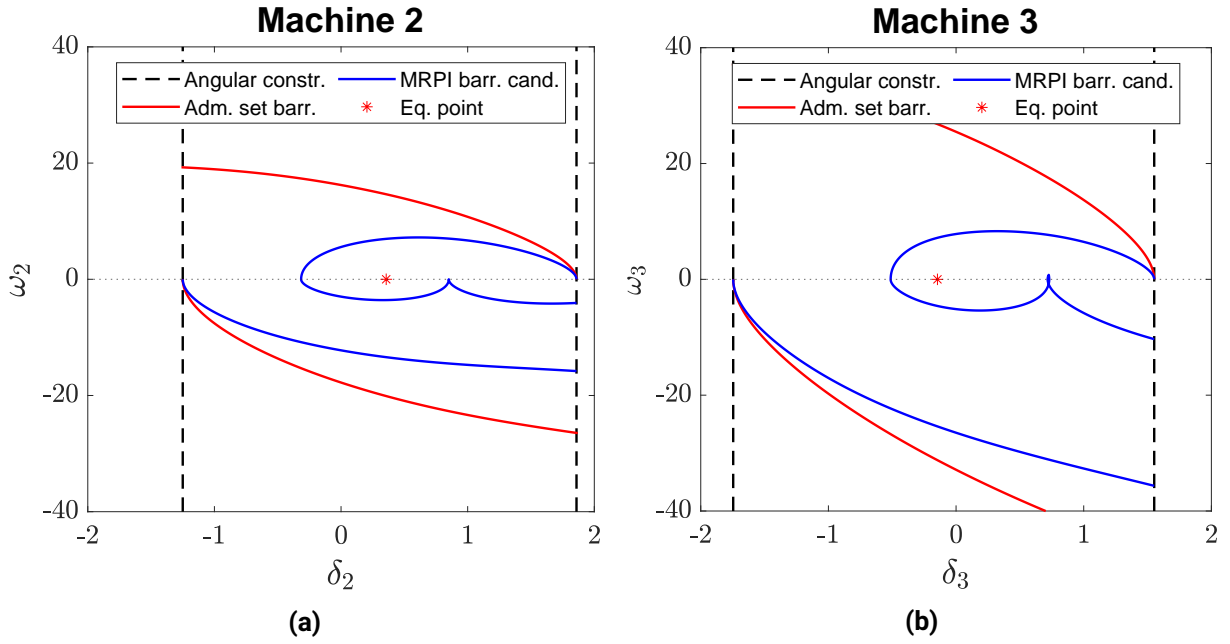


Figure 2.20: Phase diagrams of the two non-reference machines when angular constraints are $[\delta_{\min,2}, \delta_{\max,2}, \delta_{\min,3}, \delta_{\max,3}] = [\delta_{\text{eq},2}, \delta_{\text{eq},2}, \delta_{\text{eq},3}, \delta_{\text{eq},3}] + [-1.6, 1.5, -1.6, 1.7]$

Indeed, the third machine's upper MRPI barrier candidate has transitioned from phase 2 to phase 3, however, the second machine's upper barrier candidate has also transitioned from phase 6 to phase 3 as summarized in Table 2.3.

Barrier candidate	2U	2L	3U	3L
Phase	3	7	3	7

Table 2.3: Phase of each MRPI barrier candidate after decreasing $\delta_{\max,2}$ and increasing $\delta_{\max,3}$ by 0.1 rad as in Figure 2.20.

This has also been expected, because taking a look at Table 2.2 we see that relevant angular constraints are the same for both the upper angular constraints of machines 2 and 3, except in opposite directions. This approach thus won't work for finding consistent MRPI sets.

Another approach does work however, and the train of thought behind it is as follows. Changing angular constraints not listed in Table 2.2 for a given barrier candidate do not have (much) effect on the evolution of the barrier candidate in question. Thus, changing $\delta_{\min,2}$ and $\delta_{\min,3}$ do not have much immediate effect on the upper barrier candidates of either machine. Hence, we reset the initial conditions, and this time we increase $\delta_{\min,2}$ and $\delta_{\min,3}$ until we observe any state transition of the lower barrier candidates. This way, we arrive at the phase diagrams shown in Figure 2.21.

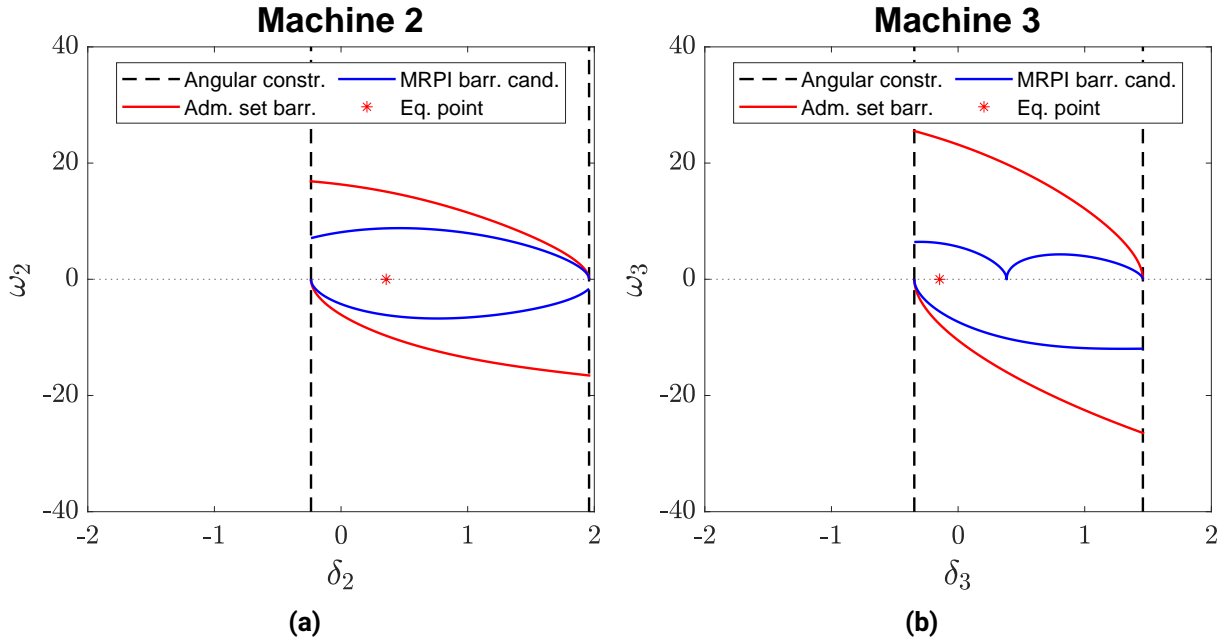


Figure 2.21: Phase diagrams of the two non-reference machines when angular constraints are $[\delta_{\min,2}, \delta_{\max,2}, \delta_{\min,3}, \delta_{\max,3}] = [\delta_{\text{eq},2}, \delta_{\text{eq},2}, \delta_{\text{eq},3}, \delta_{\text{eq},3}] + [-0.6, 1.6, -0.2, 1.6]$

Notice that the upper MRPI barrier candidates' evolution did not change by a visible amount, even though the phase 6 upper MRPI barrier candidate of machine 2 can now be considered a phase 7 MRPI barrier, due to the lower angular constraint getting closer to the equilibrium point, and intersecting the barrier in question before (going backwards in time) it would cross the $\omega = 0$ axis.

Barrier candidate	2U	2L	3U	3L
Phase	7	7	3	7

Table 2.4: Phase of each MRPI barrier candidate after increasing $\delta_{\min,2}$ and $\delta_{\min,3}$ as in Figure 2.21.

After the last modifications, we have obtained a consistent type A MRPI set for machine 2. Although this was unintentional, decreasing the distance between a machine's angular constraints is an advantageous action, because generally the narrower the interval of permitted angular deviation, the less volatile are MRPI sets as angular constraints undergo adjustment. That being said, we now re-try what resulted in Figure 2.20 before: decreasing $\delta_{\max,2}$ and increasing $\delta_{\max,3}$ so that the upper barrier candidate of machine 3 would transition towards higher phases in accordance with Table 2.2. The result is shown in Figure 2.22.

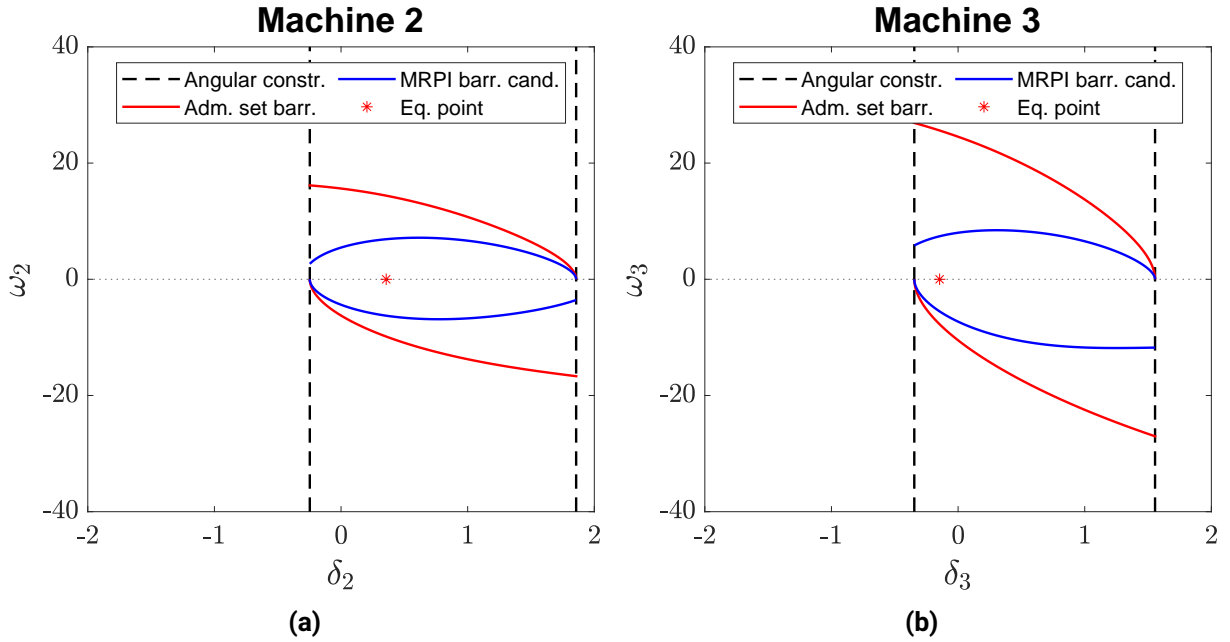


Figure 2.22: Phase diagrams of the two non-reference machines when angular constraints are $[\delta_{\min,2}, \delta_{\max,2}, \delta_{\min,3}, \delta_{\max,3}] = [\delta_{\text{eq},2}, \delta_{\text{eq},2}, \delta_{\text{eq},3}, \delta_{\text{eq},3}] + [-0.6, 1.5, -0.2, 1.7]$

Indeed, after the modifications, all barrier candidates are of phase 7, and thus both non-reference machines have a consistent type A MRPI set.

Barrier candidate	2U	2L	3U	3L
Phase	7	7	7	7

Table 2.5: Phase of each MRPI barrier candidate in accordance with Figure 2.22.

Comparing Figure 2.19(a), Figure 2.21(a) and Figure 2.22(a) we can arrive at an intuitive explanation on how it was possible to find valid phase 7 MRPI barrier candidates as we moved the lower angular constraints closer to the equilibrium point.

- First, moving the lower angular constraint closer to the equilibrium point results in the angular constraint intersecting the upper barrier candidate. Furthermore, the closer the lower angular constraint to the equilibrium point is, the higher ω_2 value the intersection will take place at.
- Then, in Figure 2.21 we have a situation in which the upper barrier candidate of machine 3 has to transition towards higher phases, but which can only be initiated by actions that would also cause the upper barrier candidate of machine 2 to transition towards lower phases. However, we now have enough leeway in the second machine's upper MRPI barrier candidate's evolution so that as the third machine's upper barrier candidate transitions to phase 6 or 7, the second machine's upper barrier candidate either remains in phase 7 or does not transition below phase 6, resulting in consistent MRPI sets for both machines.

- After the last modification to the angular constraints, we observe that as the third machine's upper MRPI barrier candidate transitioned into phase 7, the second machine's although transitioned towards phase 6 —as indicated by the lower ω_2 value at which it intersects the lower angular constraint than before the adjustment—, it just happened to remain in phase 7.

2.7 Inverse damping adjustment

Since angular constraints denote limits of safe operation of the normal operating state in Dy-Liacco's model (see Figure 1.2), they determine when the power grid transitions to the alert- or emergency operating states. In other words, they are *virtual* in the sense that they do not directly embody any physical quantities. (This constitutes a major reason for why having a method for rapid constraint re-evaluation would be advantageous, especially with the energy landscape shifting towards a more diversified, dynamically changing one as outlined in Chapter ??.)

However, the barrier phases of Section 2.4 are not only affected by angular constraints, but also by such physical quantities a mechanical damping, that is, D_i in (1.6). Even though a machine's damping is a rather fixed physical characteristic, it might still worth exploring how it affects the barrier candidates' evolution, so that an iterative process similar to that in Section 2.6 might be extended by involving the temporary adjustment of the damping coefficient.

Furthermore, it is possible, that grid topology and mechanical characteristics of the grid's elements mathematically do not allow for the existence of a valid MRPI set for each and every non-reference node. Even then, involving the damping in an interactive process similar to that in Section 2.6 can help reveal which nodes implicate damping deficiency and by what extent. This might be of good use due to advancements in researching approaches towards providing additional damping for power systems with a high share of regenerative power sources such as in [39] and [19].

To illustrate damping adjustment, we will examine machine 3 from the initial setup of Section 2.6, Figure 2.19. Although unstated, the damping coefficients in this scenario were initially provided as $D_1 = D_2 = D_3 = 50$ by [32]. This resulted in a phase 2 upper MRPI barrier candidate for machine 3 as shown in Table 2.2. However, we observe that as we increase the damping coefficient, the upper barrier candidate of machine 3 shifts towards phase 7 as shown in Figure 2.23.

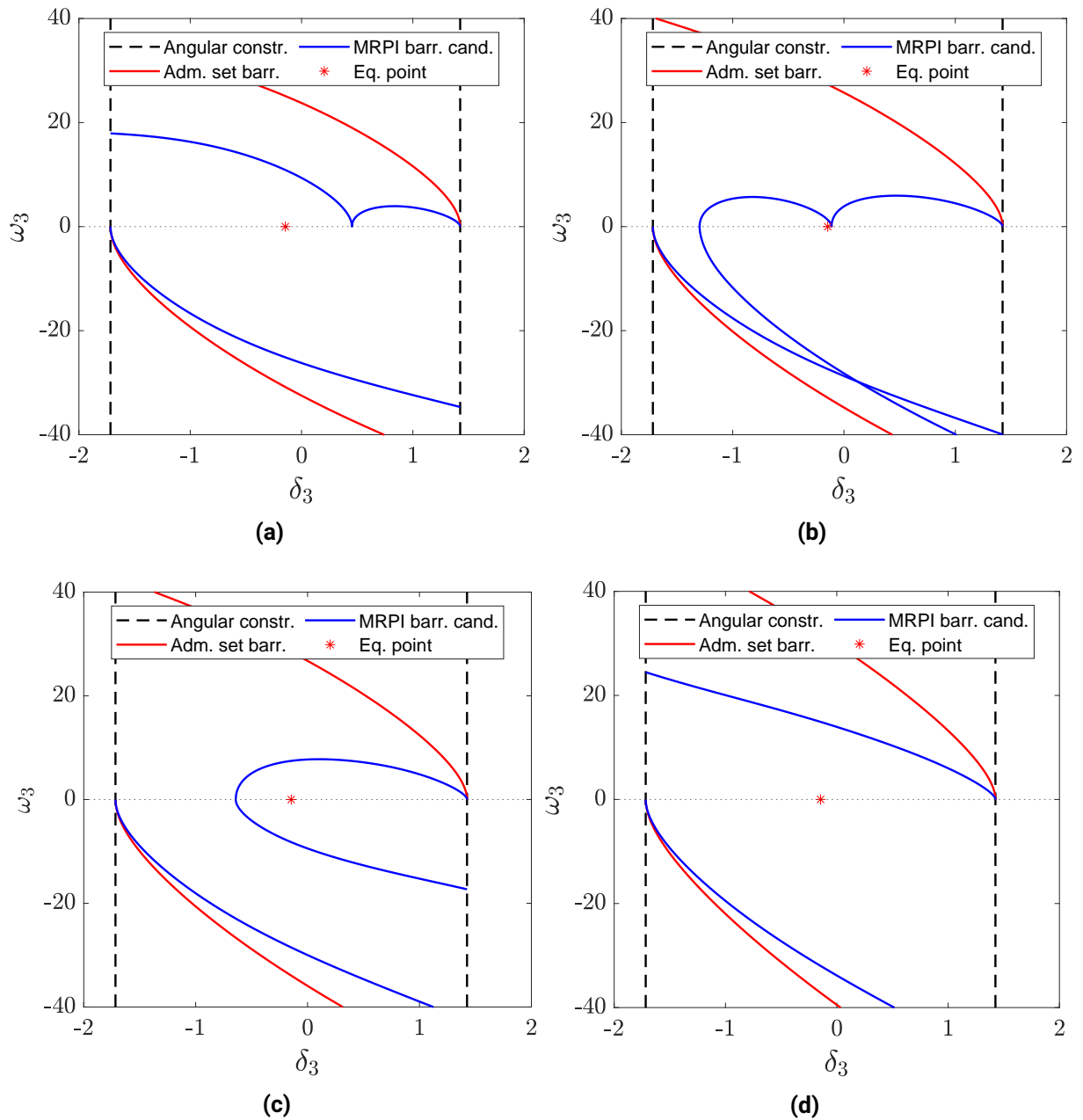


Figure 2.23: Phase diagrams of machine 3 from Figure 2.19(b), with its damping coefficient set to various values. The damping coefficient of the second machine and the reference machine was 50 in all cases. (a): $D_3 = 50$. (b): $D_3 = 60$. (c): $D_3 = 65$. (d): $D_3 = 80$.

Damping coefficient D_3	50	60	65	80
Upper MRPI barrier candidate's phase	2	3	6	7
Lower MRPI barrier candidate's phase	7	7	7	7

Table 2.6: The damping coefficient's effect on the MRPI barrier candidates' phases in accordance with Figure 2.23.

CONCLUSION AND OUTLOOK

3.1 Summary

The main intention of this work was to explore set-based transient stability analysis of power systems, as well as to lay down the groundwork for future investigation on its implementability and automatability. Particularly, the questions *“For given power grid parameters and constraints, how does one determine bounds of safe operation, and how does one redefine the latter so that safe operation of the entire grid can be granted?”* have been examined.

Chapter 1 served as an overview of the preliminaries necessary for subsequent exploratory efforts. Hereby, power system stability was defined and classified, arriving at what this work is exclusively concerned with: transient rotor angle stability. Equations governing power system operation have been presented, along with how pre-fault, fault-on, and post-fault scenarios tie in with these operating states. A prototypical use-case for transient stability analysis was briefly characterized. Approaches used for stability assessment have been surveyed: the equal areas criterion, time domain simulations, direct methods, model-free approaches, and set-based approaches. The swing equation and the power-angle relationship –together describing the fundamental dynamics of individual synchronous electrical machines– have been proposed, along with the coupled oscillator representation of power systems, including a brief overview on its historical origins. At this point, the fundamentals of viability theory were presented up to the definition of the admissible set, and the maximal robust positively invariant (MRPI) set. Then, the subsequent part deduced how –with the help of barrier theory– can above sets be determined computationally. It has been shown that complex dynamical systems such as power grids can be decoupled into subsystems, the stability assessment of which can take place individually through set-based analysis. Finally the chapter’s content so far was summarized by demonstrating how admissible-, and MRPI set barriers can be calculated in the general case, given that an oscillatory model has been built and the complete system underwent decomposition.

Chapter 2 aimed to record the research project’s progression, while documenting upcoming obstacles and peculiarities. Thus, the two topologically distinct types of valid MRPI sets of a generator have been pictured and described, along with MRPI barriers’ possible invalidities: the constraint violation and the jumping phenomenon. The theoretical explanation for why, how, and when these invalidities come to be has also been deduced. Afterwards, the description of the research framework followed: the software landscape (MATLAB with the MATPOWER library) has been introduced along with the three-machine, nine-bus system on which all subsequent tests were conducted. It has been described how experimentation with the interactive sliders helped propos-

ing the conjecture on MRPI barrier phases, in which MRPI barrier candidates tend to go through very specific stages. Said stages have each been illustrated and described, and the characteristics of each phase have been summarized in a tabular fashion. Subsequently, the one-machine-one-bus, and nine-bus test systems were utilized as a vehicle for demonstrating interdependence of angular constraints, barrier phases, and the existence of MRPI sets. An approach for finding consistent MRPI sets through iterative manual adjustment of the interactive sliders in case of the nine-bus system was shown. Lastly, it has been shown that even if no combination of angular constraints would grant sufficient stability for the whole of a given power grid, the existence of such an iterative method could still be extended by involving generator damping coefficients as adjustable parameters. This way, *damping bottlenecks* could be localized and assessed at which providing additional damping would act in favor of the whole grid's stability.

3.2 Outlook

Even though the manual process in Section 2.6 has supposed to demonstrate the applicability of the conjecture proposed in Section 2.4, further investigation in the automatability of methods built on it is still to be conducted. Questions yet to be examined include the following:

- How does one tell which phase an MRPI barrier candidate is currently in without relying on human intuition and/or in more complex systems?
- How do we computationally determine which constraints what kind (and how strong) of an effect have on MRPI barrier candidate phases?
- When machine parameters such as damping must be left unmodified, how does one go about making a statement on whether a set of angular constraints building consistent MRPI sets for all machines exist in the first place?
- What –if anything– do MRPI barrier phases imply regarding MRPI set area size? Could the proposed iterative approach be extended so that not just any MRPI sets are found, but the ones granting the most stable grid?
- What peculiarities and engineering barriers may arise while implementing an automated search algorithm or optimization problem? Is it possible to develop a computationally inexpensive and scalable solution?

Given the numerous open-ended questions, subsequent exploratory research focusing on the implementability and automatability of set-based transient stability analysis of power systems would be desirable.

BIBLIOGRAPHY

- [1] M. ALTHOFF, M. CVETKOVIC, M. ILIC, "Transient Stability Analysis by Reachable Set Computation", presented at the IEEE Power and Energy Society International Conference and Exhibition on Innovative Smart Grid Technologies, Berlin, Germany (2012).
- [2] P. M. ANDERSON, A. A. FOUAD, *Power System Control and Stability*, Hoboken, NJ, USA: Wiley (2003).
- [3] T. ASCHENBRUCK, W. ESTERHUIZEN, S. STREIF, "Transient Stability Analysis of Power Grids with Admissible and Maximal Robust Positively Invariant Sets", *Automatisierungstechnik* 68, 12 (2020), 1011–1021.
- [4] JP. AUBIN, *Viability Theory*, Cambridge, MA: Birkhäuser Boston (1991).
- [5] JP. AUBIN, A. M. BAYEN, P. SAINT-PIERRE, *Viability Theory: New Directions*, Berlin-Heidelberg, Germany: Springer (2011).
- [6] U. A. BAKSHI, M. V. BAKSHI, *Modern Control theory*, Pune, Maharashtra, India: Technical Publications (2008).
- [7] A. R. BERGEN, D. J. HILL, "A Structure Preserving Model for Power System Stability Analysis", *IEEE Transactions on Power Apparatus and Systems* 100, 1 (1981), 25-35.
- [8] F. BLANCHINI, "Set invariance in control", *Automatica* 35, 11 (1999), 1747-1767.
- [9] M. CHEN, S. L. HERBERT, M. S. VASHISHTHA, S. BANSAL, C. J. TOMLIN, "Decomposition of Reachable Sets and Tubes for a Class of Nonlinear Systems", *IEEE Transactions on Automatic Control* 63, 11 (2018), 3675–3676.
- [10] M. CHEN, S. L. HERBERT, C. J. TOMLIN, "Fast reachable set approximations via state decoupling disturbances", presented at the IEEE 55th Conference on Decision and Control (CDC), Las Vegas, NV, USA, pp. 191-196 (2016).
- [11] K. CZOLCZYNSKI, P. PERLIKOWSKI, A. STEFANSKI, T. KAPITANIAK, "Huygens' odd sympathy experiment revisited", *International Journal of Bifurcation and Chaos* 21, 7 (2011), 2047-2056.
- [12] J. H. CHOW, *Time-Scale Modeling of Dynamic Networks with Applications to Power Systems*, Berlin-Heidelberg, Germany: Springer (1982).
- [13] J. A. DONÁ, J. LÉVINE, "On barriers in state and input constrained nonlinear systems", *SIAM Journal on Control and Optimization* 51, 4 (2013), 3208-3234.
- [14] T. E. DY-LIACCO, "Control of Power Systems via the Multi-Level Concept", Ph.D. thesis, Case Western Reserve University, Cleveland, OH, USA (1968).

- [15] W. ESTERHUIZEN, T. ASCHENBRUCK, S. STREIF, "On maximal robust positively invariant sets in constrained nonlinear systems", *Automatica* 119, 109044 (2020).
- [16] G. FILATRELLA, A. H. NIELSEN, N. F. PEDERSEN, "Analysis of a power grid using a Kuramoto-like model", *The European Physical Journal B* 61, 4 (2008), 485–491.
- [17] L. H. FINK, K. CARLSEN, "Operating Under Stress and Strain", *IEEE Spectrum* 15, 3 (1978), 43–58.
- [18] L. L. GRIGSBY, J. H. HARLOW, J. D. McDONALD, *Power System Stability and Control*, Boca Raton, FL: CRC Press (2012).
- [19] H. HUANG, C. Y. CHUNG, "Coordinated Damping Control Design for DFIG-Based Wind Generation Considering Power Output Variation", *IEEE Transactions on Power Systems* 27, 4 (2012), 1916-1925.
- [20] CH. HUYGENS, Letters to R. F. de Sluse, Co. Huygens, and R. Moray, no. 1333, 1335, and 1345, The Hague, Dutch Republic (1665). Available: ckcc.huygens.knaw.nl/epistolarium/letter.html?id=huyg003/{1333,1335,1345}
- [21] L. JIN, H. LIU, R. KUMAR, J.D. MCCALLEY, N. ELIA, V. AJJARAPU, "Power system transient stability design using reachability based stability-region computation", presented at the 37th Annual North American Power Symposium, Ames, IA, USA (2005).
- [22] R. E. KÁLMÁN, J. E. BERTRAM, "Control System Analysis and Design Via the "Second Method" of Lyapunov: I—Continuous-Time Systems", *Journal of Basic Engineering* 82, 2 (1960), 371-393.
- [23] P. KUNDUR, N. J. BALU, M. G. LAUBY, *Power System Stability and Control*, New York: McGraw-Hill (1994).
- [24] Y. KURAMOTO, "Self-entrainment of a population of coupled non-linear oscillators", presented at the International Symposium on Mathematical Problems in Theoretical Physics, Kyoto, Japan (1975).
- [25] A. LI, M. CHEN, "Guaranteed-Safe Approximate Reachability via State Dependency-Based Decomposition", presented at the American Control Conference (ACC), Denver, CO, USA, pp. 1-3 (2020).
- [26] A. M. LYAPUNOV, "The general problem of the stability of motion ", Doctoral dissertation, Kharkiv University, Kharkiv, Russian Empire (1892).
- [27] A. M. MIHIRIG, "Transient stability analysis of multimachine power systems by catastrophe theory", Doctoral dissertation, University of British Columbia, Vancouver, BC, Canada (1987).
- [28] M. MOEHTAR, T. C. CHENG, L. HU, "Transient stability of power system-a survey", presented at WESCON'95, San Francisco, CA, USA, 7-9 (1995).

-
- [29] A. E. MOTTER, S. A. MYERS, M. ANGHEL, T. NISHIKAWA, "Spontaneous synchrony in power-grid networks", *Nature Physics* 9, 3 (2013), 191–197.
- [30] Z. NÉDA, E. RAVASZ, T. VICSEK, Y. BRECHET, A. L. BARABÁSI, "Physics of the rhythmic applause", *Physical Review E* 61, 6 (2000), 6987-6992.
- [31] T. NISHIKAWA, A. E. MOTTER, "Comparative analysis of existing models for power-grid synchronization", *New Journal of Physics* 17, 015012 (2015).
- [32] T. NISHIKAWA, *Power-grid synchronization models* (accessed Apr. 20, 2021) <https://sourceforge.net/projects/pg-sync-models/> .
- [33] M. PAVELLA, D. ERNST, D. RUIZ-VEGA *Transient Stability of Power Systems: A Unified Approach to Assessment and Control*, Boston, MA: Kluwer (2000).
- [34] S. J. PEALE, "Orbital Resonances in the Solar System", *Annual Review of Astronomy and Astrophysics*, 14 (1976), 215-246.
- [35] W. D. STEVENSON, *Elements of Power System Analysis*, London, UK: McGraw-Hill (1955).
- [36] S. H. STROGATZ, D. M. ABRAMS, A. MCROBIE, B. ECKHARDT, E. OTT, "Crowd synchrony on the Millennium Bridge", *Nature* 438, (2005), 43-44.
- [37] S. H. STROGATZ, "From Kuramoto to Crawford: exploring the onset of synchronization in populations of coupled oscillators", *Physica D: Nonlinear Phenomena* 143, 1–4 (2000), 1-20.
- [38] F. TORELLI, F. MILANO, A. DE BONIS, "A general power system control technique based on Lyapunov's function", presented at the IEEE 13th International Workshop on Signal Processing Advances in Wireless Communications (SPAWC), Cesme, Turkey, (2012).
- [39] S. WEI, Y. ZHOU, G. XU, Y. HUANG, "Motor-generator pair: a novel solution to provide inertia and damping for power system with high penetration of renewable energy", *IET Generation, Transmission & Distribution* 11, 7 (2017), 1839-1847.
- [40] A. T. WINFREE, "Biological rhythms and the behavior of populations of coupled oscillators", *Journal of Theoretical Biology* 16, 1 (1967), 15-42.
- [41] A. T. WINFREE, "The prehistory of the Belousov-Zhabotinsky oscillator", *Journal of Chemical Education* 61, 8 (1984), 661-663.
- [42] R. D. ZIMMERMAN, C. E. MURILLO-SÁNCHEZ, *MATPOWER User's Manual - Version 7.1*, Tempe, AZ, USA: Power Systems Engineering Research Center (2020).



TECHNISCHE UNIVERSITÄT
CHEMNITZ

Studentenservice – Zentrales Prüfungsamt
Selbstständigkeitserklärung

Name: Molnár Vorname: Gyula geb. am: <input type="text"/> Matr.-Nr.: <input type="text"/>	Bitte beachten: 1. Bitte binden Sie dieses Blatt am Ende Ihrer Arbeit ein.
--	--

Selbstständigkeitserklärung*

Ich erkläre gegenüber der Technischen Universität Chemnitz, dass ich die vorliegende **schriftliche Arbeit** selbstständig und ohne Benutzung anderer als der angegebenen Quellen und Hilfsmittel angefertigt habe.

Die vorliegende Arbeit ist frei von Plagiaten. Alle Ausführungen, die wörtlich oder inhaltlich aus anderen Schriften entnommen sind, habe ich als solche kenntlich gemacht.

Diese Arbeit wurde in gleicher oder ähnlicher Form noch nicht als Prüfungsleistung eingereicht und ist auch noch nicht veröffentlicht.

Datum: 27.08.2021

Unterschrift: 

* Statement of Authorship

I hereby certify to the Technische Universität Chemnitz that this thesis is all my own work and uses no external material other than that acknowledged in the text.

This work contains no plagiarism and all sentences or passages directly quoted from other people's work or including content derived from such work have been specifically credited to the authors and sources.

This paper has neither been submitted in the same or a similar form to any other examiner nor for the award of any other degree, nor has it previously been published.